CHALMERS
UNIVERSITY OF TECHNOLOGY

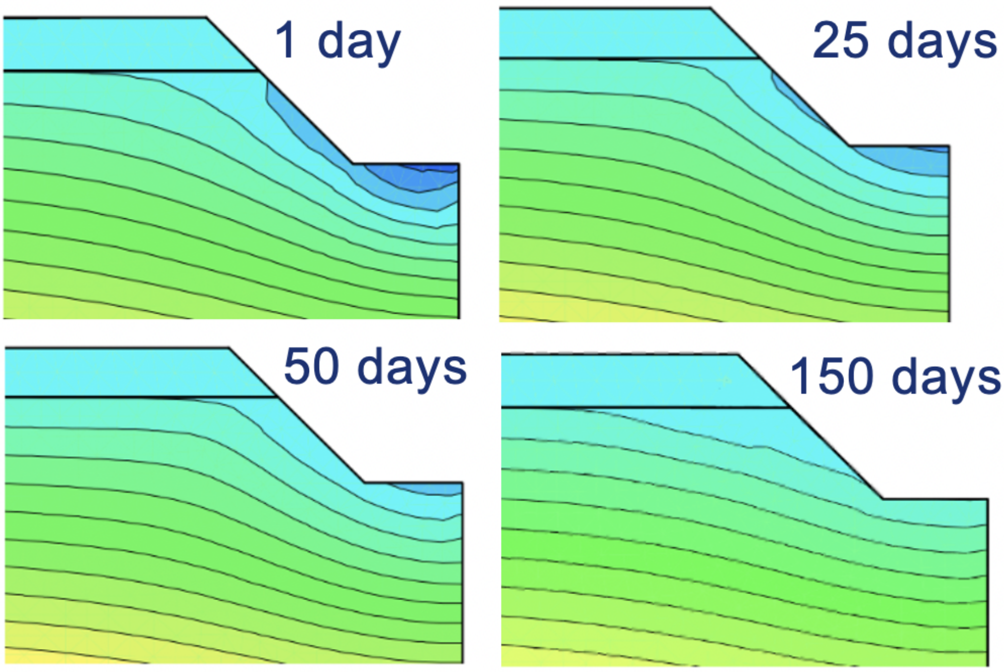

Time-dependent slope stability of temporary excavations in soft clay

A numerical study of the undrained to drained transition using combined analysis

Master's thesis in Infrastructure and Environmental Engineering

Malva Johansson
Gabriella Sanftleben

DEPARTMENT OF ARCHITECTURE AND CIVIL ENGINEERING

CHALMERS UNIVERSITY OF TECHNOLOGY
Gothenburg, Sweden 2026
www.chalmers.se

Master's thesis 2026

Time-dependent slope stability of temporary excavations in soft clay

A numerical study of the undrained to drained transition using combined analysis

Malva Johansson
Gabriella Sanftleben

Department of Architecture and Civil Engineering
Division of Geology and Geotechnics
Chalmers University of Technology
Gothenburg, Sweden 2026

Time-dependent slope stability of temporary excavations in soft clay
A numerical study of the undrained to drained transition using combined analysis
Malva Johansson
Gabriella Sanftleben

Supervisor:
Mats Karlsson, Department of Architecture and Civil Engineering, Division of Geology and Geotechnics, Chalmers.
David Nguyen, Skanska.
Viktor Lundqvist, Skanska.

Examiner: Mats Karlsson, Department of Architecture and Civil Engineering, Division of Geology and Geotechnics, Chalmers.

Master's Thesis 2026
Department of Architecture and Civil Engineering
Division Geology and Geotechnics
Chalmers University of Technology
SE-412 96 Gothenburg
Telephone +46 31 772 1000

Cover: Development of pore pressure distribution over time for a 1:1 slope inclination at 1, 25, 50 and 150 days after excavation. Further presented in Section 4.1.

Typeset in LaTeX
Gothenburg, Sweden 2026

Time-dependent slope stability of temporary excavations in soft clay
A numerical study of the undrained to drained transition using combined analysis
Malva Johansson
Gabriella Sanftleben
Department of Architecture and Civil Engineering
Division of Geology and Geotechnics
Chalmers University of Technology

Abstract

Temporary excavations in soft clay present significant stability challenges in urban infrastructure construction, especially when slopes are steep or kept open for extended periods. Current geotechnical practice assesses short-term stability using undrained analysis, an assumption that does not account for the time-dependent processes that occur as pore pressures dissipate and soil behaviour transitions from undrained to drained conditions. This transitional phase is well recognized in theory but lacks a consistent framework for practical application, which can lead to either overly conservative or insufficient stability analysis. This thesis investigates the time-dependent slope stability of temporary excavations in soft clay through combined numerical modelling. Finite Element analyses were performed in PLAXIS 2D to simulate the generation and dissipation of negative pore pressures following excavation, which were subsequently exported to SLOPE/W where Limit Equilibrium analyses were conducted to evaluate the factor of safety over time. Three slope geometries with inclinations of 1:1, 1:1,5 and 1:2 were analysed. A sensitivity analysis was further conducted to evaluate the influence of key material parameters on the results. The results show that negative excess pore pressures generated due to stress relief during excavation provide a temporary but significant stabilising contribution in short term. As consolidation progresses, these pore pressures dissipate and the factor of safety gradually converges towards long-term drained values. Slope geometry was found to govern both the magnitude and the rate of this transition: steeper slopes reach drained conditions more rapidly, while flatter slopes maintain short-term stability over longer periods. The undrained assumption was found to be valid for approximately 5 days for the 1:1 slope and 15 days for the 1:1,5 and 1:2 slopes, after which a combined analysis should be applied. The effective friction angle was identified as the most critical parameter for stability throughout the consolidation period, while the Young's modulus and permeability governs the rate of transition. The results further show that a traditional combined analysis without accounting for transient negative pore pressure underestimates short-term stability compared to the method in which distribution of pore pressure was included. Overall, the results demonstrate that the transition from undrained to drained conditions is a gradual process, and that capturing the transient pore pressure response is essential for accurately representing the temporary stabilising effect of excavations.

Keywords: temporary excavations, slope stability, combined analysis, undrained analysis, drained analysis, negative pore water pressure, time-dependent slope stability, PLAXIS 2D, SLOPE/W.

Tidsberoende släntstabilitet för temporära schakter i lös lera
En numerisk studie av övergången från odränerade till dränerade förhållanden genom kombinerad analys
Malva Johansson
Gabriella Sanftleben
Institutionen för Arkitektur och Samhällsbyggnadsteknik
Avdelningen för Geologi och Geoteknik
Chalmers Tekniska Högskola

Sammanfattning

Temporära schakter i lös lera medför betydande stabilitetsutmaningar vid byggande av urban infrastruktur, särskilt när slänter ställs branta eller hålls öppna under längre tidsperioder. Nuvarande geoteknisk praxis bedömer korttidsstabilitet med hjälp av odränerad analys, ett antagande som inte tar hänsyn till de tidsberoende processer som uppstår när portrycken jämnas ut och jordbeteendet övergår från odränerade till dränerade förhållanden. Denna övergångsfas är välkänd i teorin men saknar konsekvent ramverk för praktisk tillämpning, vilket kan leda till antingen alltför konservativa eller otillräckliga stabilitetsanalyser. Detta examensarbete undersöker den tidsberoende släntstabiliteten för temporära schakter i lera genom kombinerad numerisk modellering. Finita elementanalyser utfördes i PLAXIS 2D för att simulera generering och utjämning av negativa portryck efter schaktning, vilka sedan exporterades till SLOPE/W där Limit Equilibriumanalyser genomfördes för att utvärdera säkerhetsfaktorn med tiden. Tre släntgeometrier med lutningarna 1:1, 1:1,5 och 1:2 analyserades. En känslighetsanalys genomfördes dessutom för att utvärdera hur materialparametrar påverkar resultaten. Resultaten visar att negativa porundertryck som genereras på grund av avlastning vid schakt ger ett temporärt men betydande stabiliserande bidrag på kort tid. I takt med att konsolideringen fortgår utjämnas dessa portryck och säkerhetsfaktorn konvergerar gradvis mot långsiktiga dränerade värden. Släntgeometrin visade sig styra både storleken och hastigheten för denna övergång: brantare slänter når dränerade förhållanden snabbare, medan flackare slänter bibehåller korttidsstabilitet under längre tid. Det odränerade antagandet visade sig vara giltigt i ungefär 5 dagar för slänten med lutning 1:1, och 15 dagar för slänterna med lutning 1:1,5 och 1:2, vartefter en kombinerad analys bör tillämpas. Den effektiva friktionsvinkeln identifierades som den mest kritiska parametern för stabiliteten under hela konsolideringsperioden och E-modulen samt permeabilitet styr främst övergångshastigheten. Resultaten visar vidare att en traditionell kombinerad analys utan hänsyn till transienta negativa portryck underskattar korttidsstabiliteten jämfört med metoden där portrycksfördelning inkluderades. Sammantaget visar resultaten att övergången från odränerade till dränerade förhållanden är en gradvis process där det är viktigt att fånga den transienta portrycksresponsen för att representera temporära stabiliserande effekter från schaktning.
Nyckelord: temporära schakter, släntstabilitet, kombinerad analys, odränerad analys, dränerad analys, negativt porvattentryck, tidsberoende släntstabilitet, PLAXIS 2D, SLOPE/W.

Acknowledgements

This thesis has been conducted within the master's programme Infrastructure and Environmental Engineering at Chalmers University of Technology in Gothenburg, Sweden. More precisely, it was conducted at the division of Geology and Geotechnics, Department of Architecture and Civil Engineering. We would therefore like to thank our supervisor and examiner Mats Karlsson at Chalmers University of Technology for his feedback and advice. The thesis has been conducted in collaboration with Skanska Teknik and Skanska Väg och Anläggning in Gothenburg. We would therefore like to thank our supervisors David Nguyen and Viktor Lundqvist for their support and guidance throughout the thesis. A special thanks to Anders Kullingsjö and Torbjörn Edstam for sharing their knowledge and providing important input during the project. Finally, we would like to thank everyone we met at Skanska for their support throughout the project, their interest in our work and for creating a welcoming and enjoyable working environment.

Malva Johansson & Gabriella Sanftleben, Gothenburg, June 2026

Declaration of AI

Artificial intelligence (AI) tools were used as supportive tools during the work of this thesis. The tools were primarily used for translation between Swedish and English, grammar and language review, LaTeX formatting and table setup in Overleaf, as well as Python scripting for figure generation and data visualization. All generated material was critically reviewed, modified, and validated by the authors. The authors therefore take full responsibility for the content, accuracy, and integrity of the final work.

Contents

Nomenclature

Abbreviations

FEM	Finite Element Method
FoS	Factor of Safety
LEM	Limit Equilibrium Method
M-C	Mohr-Coulomb
OCR	Over Consolidation Ratio
SGI	Swedish Geotechnical Institute

Greek letters

$\Delta\sigma$	change in total stress	[kPa]
γ	unit weight	[kN/m^3]
γ_w	unit weight of water	[kN/m^3]
γ_{sat}	saturated unit weight	[kN/m^3]
γ_{unsat}	unsaturated unit weight	[kN/m^3]
ν	Poisson's ratio	[-]
ϕ'	effective friction angle	[$^\circ$]
ϕ^b	suction friction angle	[$^\circ$]
σ	total stress	[kPa]
σ'	effective stress	[kPa]
σ'_0	initial effective stress	[kPa]
σ'_h	effective horizontal stress	[kPa]
σ'_v	effective vertical stress	[kPa]
σ_1	major principal stress	[kPa]
σ_3	minor principal stress	[kPa]
σ_n	normal stress acting on the failure plane	[kPa]
σ_{zz}	normal stress in the out-of-plane direction	[kPa]
τ	shear stress	[kPa]
τ_f	average shear strength at failure	[kPa]
τ_{fd}	drained shear strength	[kPa]

τ_{fu}	undrained shear strength	[kPa]
τ_{mob}	mobilised shear stress	[kPa]
ε	total strain	[-]
ε^e	elastic strain	[-]
ε^p	plastic strain	[-]
ε_{zz}	strain in the out-of-plane direction	[-]
F_f	force equilibrium factor	[-]
F_m	moment equilibrium factor	[-]
h	pressure head	[m]

Roman letters

Δu	change in pore water pressure	[kPa]
ΣM_{sf}	strength reduction factor	[-]
c'	effective cohesion	[kPa]
c_u	undrained shear strength	[kPa]
c_v	coefficient of consolidation	[m^2/s]
c_{uk}	corrected undrained shear strength	[kPa]
E	Young's modulus	[kPa]
E_{50}	undrained secant modulus	[kPa]
E_{oed}	oedometer modulus	[kPa]
FoS	factor of safety	[-]
G	shear modulus	[kPa]
H	drainage length	[m]
H_{exc}	excavation depth	[m]
k	permeability	[m/s]
K_0	earth pressure coefficient at rest	[-]
k_x	horizontal permeability	[m/s]
k_y	vertical permeability	[m/s]
M	oedometer modulus	[kPa]
M_0	compression modulus if $\sigma'_c > (\Delta\sigma + \sigma'_0)$	[kPa]
M_L	compression modulus if $\sigma'_c < (\Delta\sigma + \sigma'_0)$	[kPa]
s	shear strength	[kPa]
t	time after excavation	[days]
T_v	time factor	[-]
u	pore water pressure	[kPa]
u_a	pore air pressure	[kPa]

u_e	excess pore water pressure	[kPa]
u_s	static (hydrostatic) pore water pressure	[kPa]
x	distance along slip surface	[m]
y	vertical coordinate	[m]

List of Figures

List of Tables

1
Introduction

Urban development and expansion of infrastructure are increasingly requiring construction activities to be carried out in urban areas (Tornborg, 2024). In many construction projects, temporary excavations are necessary for foundations, utility installations or underground structures. Such excavations often present significant stability challenges, particularly when slopes are steep or when excavation stages remain open for extended periods (Sabattini et al., 2024). In current geotechnical practice, the short-term stability of temporary excavations in soft clay is typically evaluated using undrained analysis (SGI, 2023). This approach is based on the assumption that the soil response immediately following excavation is governed by undrained behavior. Although this assumption is appropriate for the initial stage after excavation, it does not account for the time-dependent processes that occur as the construction progresses.

Excavation unloads the ground which generates negative excess pore pressures within the slope and beneath the excavation bottom (Eigenbrod, 1974). These negative excess pore pressures gradually dissipate as drainage occurs, leading to time-dependent changes in effective stresses and shear strength (Craig, 2004). Consequently, the soil response gradually transitions from undrained to partially and fully drained. Although this behaviour is well known in geotechnical engineering, its effects on excavation stability are often only considered indirectly through the use of limiting cases, such as fully undrained or fully drained analyses. In particular, there is limited guidance regarding how long undrained assumptions remain valid or how stability should be assessed during the transitional phase.

How time dependent effects are accounted for in stability assessments can have a significant influence on the design of temporary excavations in soft clay. Conservative or simplified assumptions may result in overly restrictive or excessive support measures, leading to increased construction efforts, higher material consumption and associated environmental impacts. In practice, this may involve the implementation of extensive temporary support systems for excavations that are only required to remain open for a limited period, even though a more detailed consideration of time-dependent effects could allow for less intrusive solutions. Conversely, insufficient consideration of time effects may lead to an underestimation of stability demands and an increased risk of instability which could cause danger to people working in and around the excavation.

To address this uncertainty, a combined stability analysis could be applied, in which the shear strength of cohesive soils is defined as the minimum of the undrained and drained strengths (SGI, 2023). This approach allows the governing shear strength, and consequently the factor of safety, to vary over time as excess pore pressures dissipate and soil behavior transitions from undrained to drained conditions, thereby providing an understanding of the soil response from a time-dependent perspective.

1.1 Aim

The purpose of this thesis is to quantify how the stability of clay excavations changes with time, by considering the gradual dissipation of negative pore pressure through numerical and analytical modeling. The project specifically aims to identify how long a soft clay can realistically be considered undrained and quantify how the factor of safety changes as partial consolidation and drainage develop over time. Furthermore, the study aims to relate this time-dependent behaviour to conventional undrained, drained and combined stability analysis, in order to evaluate when a combined analysis is appropriate for the assessment of excavation stability in soft clay. The results are intended to improve safety assessments and design choices regarding temporary excavations in soft clays.

1.2 Objectives

The project will address the following key questions:

- How does pore pressure dissipate with time following slope excavation in soft clay?
- For how long after excavation does the undrained assumption remain valid for soft clay slopes, and when does a combined stability analysis become more appropriate?
- How does the factor of safety vary with the time during the transition from undrained to drained conditions?

1.3 Limitations

The study is limited to a selected range of soil conditions and excavation geometries chosen to be representative of soft clays commonly encountered in Sweden, and the results should therefore be interpreted in terms of general trends rather than project-specific predictions. The numerical analyses are confined to finite element modelling in PLAXIS 2D and limit equilibrium analyses in GeoStudio (SLOPE/W), conducted under two-dimensional plane strain conditions. The soil behaviour was limited to be modeled using Mohr-Coulomb constitutive model and the clay was assumed to be homogeneous and isotropic. External environmental effects, such as frost and rainfall were not considered in the analyses.

2
Theory

The following chapter provides the theoretical background necessary to understand the behaviour of soft clay during excavation and the time-dependent processes governing slope stability. The chapter begins by introducing the geotechnical characteristics of soft clay, followed by a description of the effective stress and pore pressure behaviour, shear strength under drained and undrained conditions, and the role of compressibility and consolidation. Slope stability theory is then presented alongside the combined stability analysis approach. The chapter concludes with an overview of the numerical and analytical tools used in this study, PLAXIS 2D and SLOPE/W. Together, these theoretical concepts form the basis for the modelling approach and the interpretation of results presented in subsequent chapters.

2.1 Geotechnical characteristics of soft clay

Soft soils and particularly soft clays are composed of fine-grained mineral particles formed through chemical weathering of bedrock material (Terzaghi, 1943). These particles have the shape of a plate and possess a high specific surface area which makes their mechanical behaviour strongly influenced by surface forces rather than direct grain to grain contact.

Unlike coarse-grained soils where particle interaction is governed primarily by friction, clay particles are held together by molecular forces acting at their surface (Sällfors, 2013). This leads to a soil structure characterised by a relatively high void ratio and a strong dependency on the presence and distribution of pore water. The high void ratio and water content result in a lower stiffness and large deformations (Larsson, 2008). The voids in the soil mass are filled with water and in some cases air (Craig, 2004), which is forming a coupled system in which the soil skeleton and pore fluid together control the response to loading. As a result, soft clays generally exhibit high compressibility and low permeability, meaning that changes in pore pressures can significantly influence effective stresses and soil behaviour (Larsson, 2008). However, the geotechnical properties of clay are primarily controlled by its structure and stress history rather than by the size of the individual particles. This cohesion arises from negative pore water pressure called capillary tension, in the small voids between particles, which create bonding forces within the soil structure (Craig, 2004). However, this cohesion may be reduced if the clay becomes fully submerged in water. Clay is also characterised by plasticity which is defined as the ability to undergo permanent deformation without cracking or crumbling (Andrade et al., 2011).

The mechanical behavior of soft clay is governed by its fabric and structure developed during deposition and subsequent geological processes. The orientation of clay particles results in anisotropic behavior (Craig, 2004), meaning that strength and deformation properties vary with direction. The stress history of the soil further controls its response to loading (Larsson, 2008). Normally consolidated clays are highly compressible and tend to generate significant excess pore pressure under load increments, whereas overconsolidated clays generally exhibit stiffer behavior and may dilate during shearing (Larsson, 2008).

Deformation in soft soils involves changes in both volume and shape and occurs as a result of particle rearrangement and the redistribution of interparticle forces (Larsson, 2008). Because clay particles are very small and the pore network is poorly connected, permeability is typically low (Terzaghi, 1943). As a result, stress changes disturb the pore water equilibrium and generate excess pore pressures, whose dissipation governs the time-dependent behaviour of the soil. The rate of pore water flow therefore directly influences the development of deformations and effective stress. This time-dependent increase in effective stress associated with dissipation of excess pore water pressure is referred to as consolidation (Knappett & Craig, 2012). In soft clays, consolidation governs settlement development and long-term stability behaviour.

2.2 Effective stress and pore pressure behaviour

The mechanical behaviour of saturated soils is governed by the principle of effective stress, originally introduced by Terzaghi (1943). The principle states that soil deformation and shear strength are controlled by the stress transmitted through the soil skeleton rather than by the total stress acting on the soil mass. When a load is applied to a saturated soil the total stress is carried by both the pore water and the grain skeleton. The pressure in the pore water acts equally in all directions while the soil deformations are governed by the contact forces between the soil grains (Verruijt, 2017). The effective stress is defined as:

$$\sigma' = \sigma - u \tag{2.1}$$

where σ' is the effective stress, σ is the total stress and u is the pore water pressure (Verruijt, 2017). The pore water pressure represents the portion of the total stress that is carried by the pore water, while the effective stress represents the portion carried by the soil grain skeleton. As described by Sällfors (2013), the effective stress governs the interparticle contact forces.

The distinction between total stress and effective stress is closely related to the drainage conditions of the soil (Sabattini et al., 2024). In undrained conditions, typically associated with short-term behaviour in low-permeability soils, the soil is often analysed using total stress. In such cases, pore water pressures are not explicitly considered, and the soil response is described using undrained shear strength parameters. In contrast, under drained conditions, which represent long-term behaviour, effective stress analysis is used. In this case, pore water pressure is explicitly accounted for, and the soil behaviour is described using effective stress and corresponding strength parameters. The choice between total and effective stress analysis therefore depends on whether the soil response is dominated by short-term undrained conditions or long-term drained conditions.

2.3 Shear strength of soft soil

The shear strength of a soil is defined as the internal resistance of a soil mass to shear stresses acting along a potential failure plane and represents the ability of the soil to withstand shear stresses before failure occurs. The shear strength depends on several factors, such as the stress state at failure, stress history, loading rate, drainage conditions and cementation (Sällfors, 2013). It is generated by resistance mechanisms acting on particle level, mainly through friction between particles but also through bonding forces and cohesion between them, where the frictional component is governed by contact forces that develop as a consequence of the effective stress acting within the soil (Larsson, 2008).

Depending on the loading or unloading conditions and the consolidation behaviour of the soil, shear strength is generally classified as undrained or drained (Larsson, 2008). In soils like sand and gravels, the pore pressure dissipation occurs rapidly due to high permeability, and the shear strength is therefore generally evaluated under drained conditions. In contrast, fine-grained soils like clay, exhibit low permeability, which causes excess pore pressure to develop and persist following loading or unloading. Under these conditions, short-term response of the soil is governed by undrained shear strength. With time, the governing shear resistance progressively shifts towards the drained shear strength, which is adopted for the assessment of long-term stability (Larsson, 2008).

2.3.1 Drained shear strength

Drained shear strength describes the shear resistance of soil when loading occurs sufficiently slowly to allow volume change and redistribution of stresses within the soil skeleton. Under these conditions, the shear strength is governed by effective stress parameters and is expressed as a function of the effective normal stress acting on a potential failure plane (Larsson, 2008). Based on the stress-strength concept introduced by Mohr, failure in soil occurs when the combination of principal stresses σ'_1 and σ'_3 generates shear stresses that reach a critical level on the failure plane (Sällfors, 2013). This relationship is commonly represented by the Mohr-Coulomb failure criterion, which is used to describe the drained behaviour of soils, shown in Equation 2.2. The corresponding Mohr-Coulomb yield surface in principal stress space is illustrated in Figure 2.1.

$$\tau_f d = c' + \sigma' \tan \phi' \tag{2.2}$$

where c' is the effective cohesion, σ' is the effective normal stress and ϕ' is the effective friction angle (Craig, 2004).

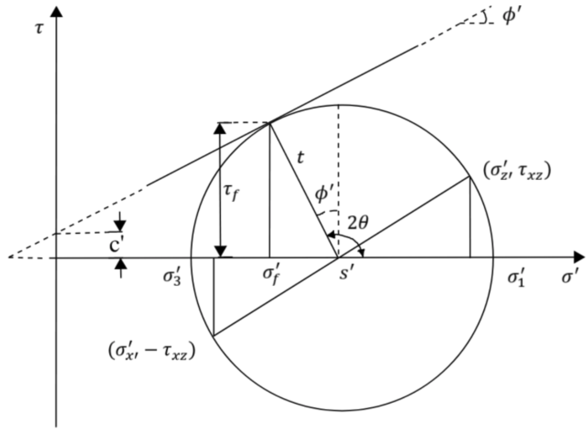

Figure 2.1: Mohr-Coulomb in principal stress space, based on (Craig, 2004)

For clay, the effective stress parameters c' and ϕ' should be regarded as representative values valid within a limited stress range rather than unique material properties. Experimental studies on Scandinavian clays have shown that the effective cohesion is generally small, with reported values typically ranging between 0-4 kPa, while the effective friction angle is relatively constant and commonly lies between approximately 25 and 33 degrees (Larsson, 1983). It should further be noted that the effective stress failure envelope for clay is not strictly linear over the entire stress range, but may exhibit a slight curvature (Larsson, 1983).

In Swedish geotechnical practice, empirical relationships could be used to relate undrained and drained shear strength parameters. The drained shear strength of cohesive soils can be estimated using the Mohr-Coulomb failure criterion given in Equation 2.2. For cohesive soils typical of Swedish conditions, the friction angle is commonly set to ϕ'=30°, while the effective cohesion can be estimated as $c' = 0.1c_u$, where c_u is the undrained shear strength (Larsson et al., 2007; Skredkommissionen, 1995; Trafikverket, 2011).

2.3.2 Undrained shear strength

Undrained shear strength, c_u, describes the shear resistance of soil under undrained conditions, where loading or unloading occurs without significant dissipation of pore water pressure (SGI, 2023). In excavation problems, stress changes are induced by the removal of overburden and the associated redistribution of stresses within the soil mass. This behaviour is particularly relevant for fine-grained soils such as clay, where the low permeability results in an undrained response immediately following excavation (Larsson, 1983).

During excavation in clay, unloading causes an immediate change in stresses within the soil mass. These stress changes create pore pressure variations, where negative pore pressures (suction) develop as a result (Sabattini et al., 2024). The pore pressure response initially balances out the change in total stress and causing the soil to behave under undrained conditions. As long as negative pore pressure persist, the stability could be assessed using undrained shear strength (Eigenbrod, 1974).

In undrained analysis, the shear strength is commonly idealised as being independent of the effective stress, which is often expressed by assuming a friction angle equal to zero. The undrained shear strength is then described as a constant value for a given soil layer according to:

$$\tau_{fu} = c_u \tag{2.3}$$

The assumption of a constant undrained shear strength with regard to effective stress is a practical idealisation that is valid for a specific depth and stress state. The magnitude of c_u is primarily governed by stress history of the soil, in particular the preconsolidation pressure (Larsson, 2008). When the major principal stress is vertical, as is typically the case in situ prior to excavation, the preconsolidation pressure controls the shear stress level at which failure occurs and thus the magnitude of undrained shear strength. If the major principal stress acts in another direction, the corresponding effective stress perpendicular to the direction of shearing governs the shear strength (Larsson, 2008).

As the yield stresses vary with direction, the undrained shear strength exhibits anisotropy. It is therefore common to distinguish between undrained shear strength in active shearing, where the major principal stress is vertical, passive shearing, where the major principal stress is horizontal, and direct shearing along a horizontal failure plane (Larsson, 2008; Larsson et al., 2007) see Figure 2.2. In slope failures, different shearing modes may develop along the failure surface and the undrained shear strength from direct shear is therefore commonly used as a representative average in simplified stability analyses. However, the influence of anisotropy becomes more pronounced in steep slopes where the active zone dominate the failure mechanisms (Skredkommissionen, 1995), whereas in flatter slopes with more balanced active and passive zones, the effect on the factor of safety is more moderate.

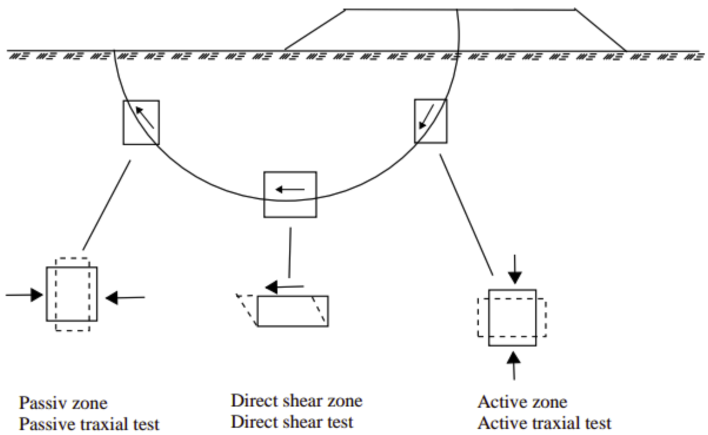

Figure 2.2: Active, passive and direct shearing, based on (Skredkommissionen, 1995)

2.4 Saturated and unsaturated soil conditions

Soil consists of solid particles and voids that may be filled with water and/or air (Craig, 2004). When all voids are completely filled with water, the soil is considered saturated. If the voids contain both water and air the soil is unsaturated. This means that part of the pore space is filled with water while the remaining part is occupied by air, see Figure 2.3.

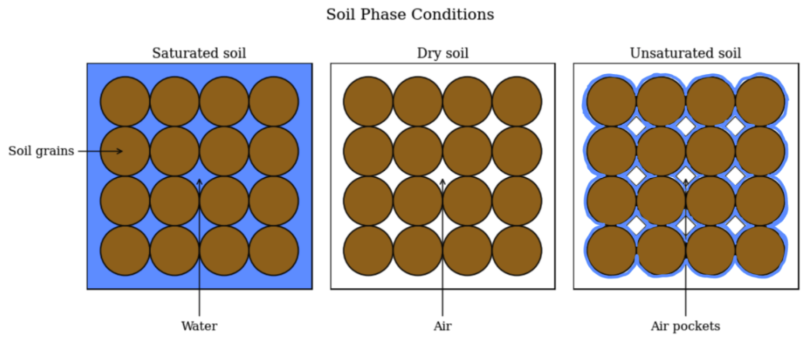

Figure 2.3: Fully saturated, dry and unsaturated, based on (VJ Tech, 2024).

The distinction between saturated and unsaturated soil refers only to the distribution of water and air within the soil and should not be confused with drained and undrained conditions. Drained and undrained behaviour instead describe whether pore water pressures dissipate or remain unchanged during loading (Craig, 2004). Below the groundwater table the pore pressure is positive, while above it, where the soil is unsaturated, the pore pressure is below atmospheric pressure and negative in value, commonly referred to as soil suction (Abramson et al., 2002).

2.4.1 Pore water pressure in saturated soils

Pore water pressure in saturated soil consist of two component:

$$u = u_s + u_e \tag{2.4}$$

where u_s is the static (hydrostatic) pore pressure and u_e is the excess pore water pressure (Craig, 2004). The static pore pressure is governed by groundwater conditions and varies with depth according to hydrostatic equilibrium. Excess pore pressure arises when total stresses change more rapidly than drainage can occur. The reduction of excess pore water pressure is referred to as dissipation. When dissipation is complete ($u_e = 0$) the soil is considered to be in a drained condition, where on the other hand the presence of excess pore water pressure indicates undrained behaviour. It is important to note that a drained condition does not mean that water has left the soil, but rather that the pore water pressure is no longer influenced by changes in stress. Instead it is controlled by groundwater conditions and throughout this process the soil remains fully saturated (Craig, 2004).

2.4.2 Pore water pressure in unsaturated soils

In unsaturated soils, the pore space contains both water and air which leads to more complex pore pressure conditions compared to saturated soils. Instead of just pore water pressure both pore air pressure u_a and pore water pressure u_w must be considered (Fredlund, 1989). The quantity $(u_a - u_w)$ is referred to as matric suction. Matric suction arises due to capillary effects and the interaction between air and water within the pore space. In unsaturated soils, the stress state can be described using two independent stress variables: the net normal stress $(\sigma - u_a)$ and the matric suction (Fredlund, 1989).

Based on this formulation, the shear strength of unsaturated soils can be expressed using an extended Mohr–Coulomb failure criterion:

$$s = c' + (\sigma_n - u_a)\tan\phi' + (u_a - u_w)\tan\phi^b \tag{2.5}$$

In this expression, the first two terms correspond to the conventional Mohr–Coulomb formulation, while the third term represents the contribution from matric suction. This term accounts for the increase in shear strength associated with negative pore water pressure. The parameter ϕ^b describes the rate of increase in shear strength with respect to matric suction and may be interpreted as a frictional component related to suction (Fredlund, 1989). The pore-air pressure is taken as atmospheric pressure ($u_a = 0$), implying that pressures are expressed relative to atmospheric conditions. This allows the suction term to be directly expressed in terms of the pore water pressure. Furthermore, the angle ϕ^b may be assumed equal or smaller than the effective friction angle ϕ'. However, it should be noted that ϕ^b is not a constant material property but varies with degree of saturation and level of matric suction. At low suction levels the soil remains nearly saturated and ϕ^b may be assumed closer to equal to ϕ', whereas at higher suction levels, ϕ^b typically decreases (Rajamanthri & Zapata, 2025). Tests have shown that the relationship between shear strength and matric suction is non-linear over a wide range of suction levels, meaning that ϕ^b changes depending on the magnitude of suction (Fredlund & Vanapalli, 2002). As saturation is approached, the pore air pressure u_a becomes equal to the pore water pressure u_w, and the matric suction term vanishes. The relationship is illustrated in Figure 2.4 where the shear strength of unsaturated soils is represented as a planar surface defined by the net normal stress and the matric suction. Figure 2.5 shows how an increase in matric suction results in an increase in shear strength, which is reflected by the inclination of the surface in the suction direction.

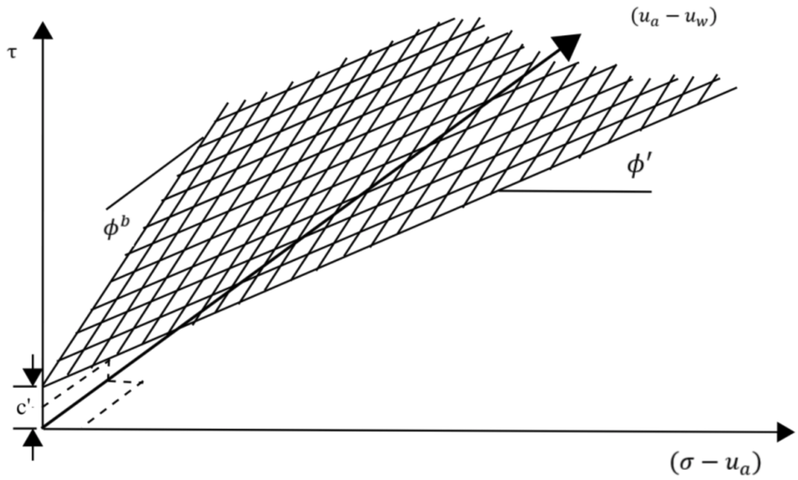

Figure 2.4: A planar representation of the shear strength relationship for unsaturated soils, based on (Fredlund, 1989).

The friction angle ϕ^b corresponds to the slope of the relationship between shear strength and matric suction when the net normal stress is kept constant. The effective angle ϕ' is assumed to remain constant for different suction levels as the failure envelope is considered to be planar. The stress conditions at failure can be represented using Mohr circles in a three-dimensional space (Figure 2.5) where the two stress state variables are plotted along the horizontal axes and the shear strength is represented on the vertical axis (Fredlund, 1989).

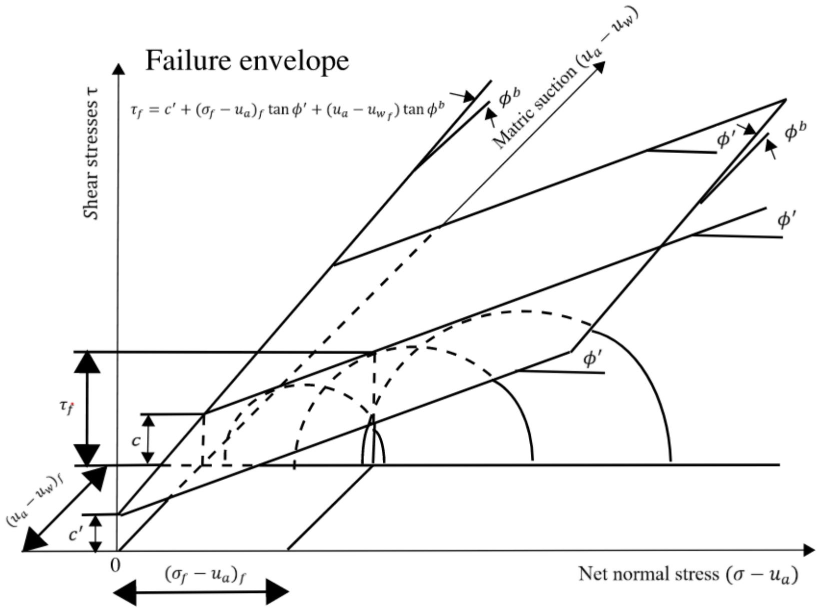

Figure 2.5: Mohr circles at failure for an unsaturated soil, based on (Fredlund, 1989).

2.4.3 Pore pressure response to excavation

Excavation causes a reduction in total stress due to removal of overburden (Craig, 2004). If the excavation occurs rapidly relative to the permeability of the clay, drainage cannot take place immediately and unloading therefore induces an undrained response (Knappett & Craig, 2012).

As a result of unloading during excavation, a temporary reduction in pore water pressure i.e. negative excess pore water pressure develops within the soil mass (Sabattini et al., 2024). This pore pressure change reflects the redistribution of stresses, where the decrease in total stress is momentarily balanced by a corresponding decrease in pore water pressure. The magnitude and distribution of the pore pressure change depend on the geometry of the excavation. At the base of the excavation, the pore pressure change is primarily governed by vertical unloading whereas near the slope it is influenced by horizontal stress relief (Sabattini et al., 2024).

Immediately after excavation negative pore water pressure develop both beneath the excavation and within the slope. This temporary suction leads to an increase in shear strength, which contributes to higher short-term stability (Sabattini et al., 2024). The stress redistribution also results in the development of active and passive zones within the soil mass. Near the slope crest, an active zone develops where the effective horizontal stress is reduced, whereas a passive zone develops closer to the toe of the slope, where the effective vertical stress is reduced (Larsson et al., 2007). These zones are associated with different stress paths and corresponding pore pressure changes, as illustrated in 2.6. In Figure 2.6, the change in pore water pressure is denoted as Δu, which corresponds to the excess pore water pressure generated immediately after excavation due to the undrained unloading of the soil (Sabattini et al., 2024). The dashed stress path represents drained conditions whereas the solid stress path represents undrained conditions.

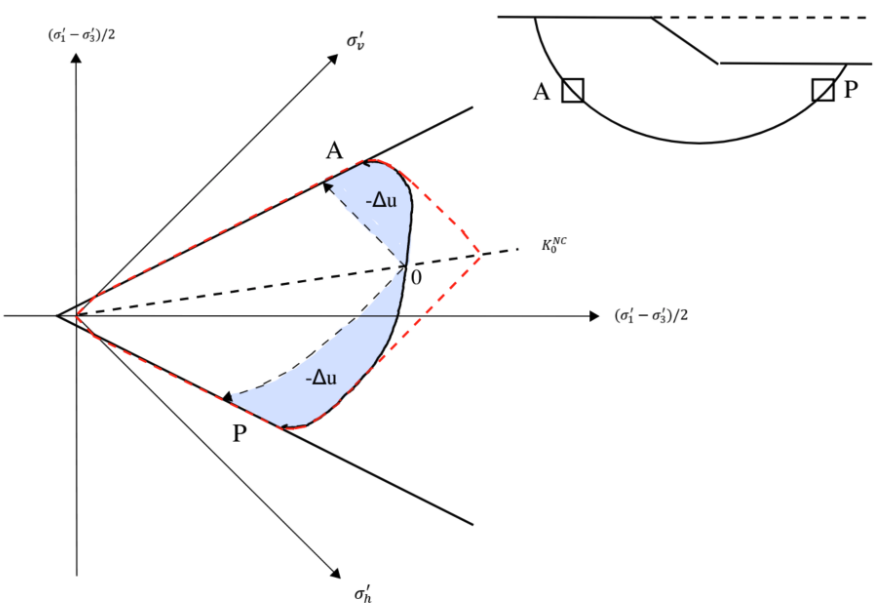

Figure 2.6: Effective stress paths associated with active and passive shear along a potential slip surface in lightly overconsolidated clay, based on (Sabattini et al., 2024). The Figure illustrates how reductions in horizontal and vertical effective stresses give rise to different stress paths and associated negative pore water pressures following excavation.

2.5 Compressibility and consolidation

When soil is subjected to a change in effective stress, it responds by changing volume. The magnitude and rate of this volume change are governed by the soil's compressibility and hydraulic conductivity (Larsson, 2008). In fine-grained soils such as clay, these properties together control the time-dependent mechanical response of the soil.

2.5.1 Compressibility

The compressibility of a soil describes its tendency to decrease in volume under an applied effective stress (Larsson, 2008). A key stiffness parameter is the constrained modulus M, which describes the relationship between compression and effective vertical stress under conditions of zero lateral strain. The magnitude of M depends on the stress history of the soil, characterized by the preconsolidation pressure σ_c' and the overconsolidation ratio $OCR = \sigma_c'/\sigma_0'$. If the effective stress generated by a new load $(\Delta\sigma + \sigma_0')$ remains below the preconsolidation pressure, the soil deforms primarily elastically and the stiffness is described by M_0. If the stress exceeds the preconsolidation pressure, the soil undergoes plastic compression and the stiffness is instead described by M_L, which is considerably lower. Both M_0 and M_L are simplified linear approximations of the stress-strain relationship and are typically assessed using CRS or incremental loading oedometer tests (Larsson, 1983). In practical geotechnical applications, soil stiffness is often estimated empirically from the undrained shear strength c_u. Figure 2.7 illustrates the definition of the secant modulus E_{50}, which is determined from the slope of the line connecting the origin and the point correspondning to 50% of the failure stress.

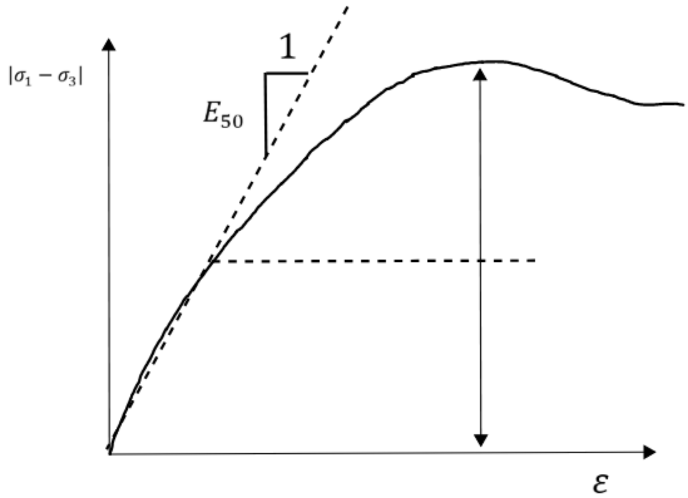

Figure 2.7: Modulus E_{50} based on (Bentley Systems, 2025a)

According to TK Geo 11 (Trafikverket, 2011), the undrained secant modulus E_{50} may be estimated based on soil type and undrained shear strength. Suggested relationships include:

$E_{50} = 1000c_u$	for silty clay
$E_{50} = 500c_u$	for low-plastic clay
$E_{50} = 250c_u$	for highly plastic clay and organic clay
$E_{50} = 150c_u$	for gyttja

In PLAXIS 2D, the oedometer stiffness E_{oed} and the secant stiffness E_{50} can be assumed to be equal for soft soils (Bentley Systems, 2025a).

2.5.2 Consolidation

Consolidation is a time-dependent process in which soil undergoes volume change as excess pore water pressure dissipates and the load gradually transferred to the soil skeleton (Sällfors, 2013). In fine-grained soils such as clay, consolidation occurs slowly due to low permeability. The rate of consolidation is governed by soil properties and drainage conditions. A key parameter is the coefficient of consolidation c_v, see Equation (2.7) which represent the combined influence of soil hydraulic conductivity and compressibility and controls how quickly excess pore water pressure dissipates (Sällfors, 2013). According to Terzaghi´s theory of one-dimensional consolidation, the dissipation of excess pore water pressure is governed by the equation:

$$\frac{\partial u_e}{\partial t} = c_v \frac{\partial^2 u_e}{\partial z^2} \tag{2.6}$$

which describes how pore pressure varies with time and depth (Knappett & Craig, 2012). The equation shows that the rate of change of excess pore water pressure with time is proportional to the curvature of the pore pressure distribution in space and controlled by the coefficient of consolidation, expressed as:

$$c_v = \frac{k\,E}{\gamma_w}\ [\mathrm{m}^2\,\mathrm{s}^{-1}] \tag{2.7}$$

where k is the hydraulic conductivity, E is the constrained modulus of the soil and γ_w is the unit weight of water (Terzaghi, 1943).

2.5.3 Time factor

To simplify the solution of Terzaghi´s consolidation equation, a dimensionless time parameter known as the time factor, T_v, is introduced (Terzaghi, 1943). The time factor expresses the relationship between elapsed time, soil properties and drainage length and allow consolidation behavior to be described independently of scale:

$$T_v = \frac{c_v\,t}{H^2} \tag{2.8}$$

where t denotes the time after excavation and H is the drainage length. The drainage length defines the distance pore water must travel to reach a drainage boundary and therefore has a direct influence on consolidation time. Since the time factor scales with the square of the drainage length, the assumed value of H strongly affects the predicted rate of pore pressure dissipation following excavation (Terzaghi, 1943).

2.6 Slope stability theory

Under normal conditions, when no failure occurs, a slope is in a state of equilibrium where the driving forces are balanced by the resisting forces within the soil mass and the slope remains stable (SGI, 2023). Changes in geometry, such as excavation or filling, disturb this equilibrium by altering the stress distribution in the slope. As a result, shear strength is mobilized along potential failure surfaces in order to establish a new balance (Craig, 2004). Stability conditions may further evolve over time due to changes in soil strength or additional loads acting on the soil making slopes formed by excavation particularly sensitive to stress distribution.

2.6.1 Slip surface geometry

The location and shape of the critical failure surface are governed by the slope geometry, loading conditions, soil stratigraphy and the variation of shear strength and pore water pressure (Craig, 2004). Based on these factors, different failure mechanisms may develop in excavation slopes, which are commonly classified according to the geometry of the slip surface. The three most commonly occurring failure modes are illustrated in Figure 2.8: rotational, translational and compound failure (Sällfors, 2013).

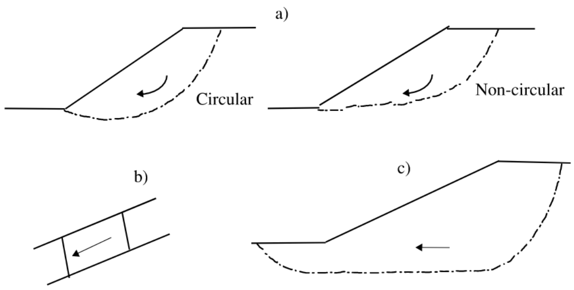

Figure 2.8: a) Rotational, b) translational, and c) compound failure, based on (Sällfors, 2013)

Translational failure

Translational failure occurs when the shape of the slip surface is distorted by a soil layer or zone with significantly different shear strength compared to the surrounding material (Craig, 2004). Such failures typically develop along weak planes, weakness zones or pre-existing discontinuities, resulting in a predominantly planar slip surface. Translational slips tends to occur where the controlling weak layer is located at a relatively shallow depth below the slope surface and the failure surface is therefore often approximately parallel to the slope inclination. In excavation slopes, translational failure may develop along interfaces between soil layers, along drainage layers, or along zones with elevated pore water pressure or reduced shear strength.

Rotational failure

Rotational failure is a common failure mechanism in clay slopes and excavations and is characterized by a slip surface that is curved and often approximated as circular in cross-section (Craig, 2004). Such failures are typically associated with relatively homogeneous and isotropic soil conditions, where shear strength and pore water pressure vary gradually with depth (SGI, 2023). However, when soil conditions are non-homogeneous, rotational failure surfaces may deviate from a perfect circular shape and become non-circular (Craig, 2004). Such non-circular rotational failures are more common in stratified soil profiles, where variations in material properties, strength contrasts or pore pressure conditions influence the geometry of the slip surface. In slopes formed in thick deposits of soft clay, failure is therefore often assumed to occur by rotation of soil mass along a circular-cylindrical slip surface.

Compound failure

Compound failure occurs when the failure surface consists of both curved and planar sections, combining characteristics of rotational and translational slips (Craig, 2004). Such failures typically develop when pronounced stratigraphic contrasts, weak layers or zones of elevated pore water pressure exist at depth causing the slip surface to follow these interfaces rather than forming a purely circular shape. In slopes that are long relative to the soil thickness a circular-cylindric slip surface may not adequately represent the most critical failure mechanism and a compound slip surface of arbitrary shape provides a more realistic description of the soil behavior (Sällfors, 2013).

2.7 Factor of safety

In classical slope stability analysis, the equilibrium of a potential sliding mass is evaluated along an assumed failure surface. The analysis may be based on force equilibrium, moment equilibrium or a combination of both (Alén et al., 2000). The driving force acting on a slope mainly consist of the self-weight of the soil or external loads while the resistance is provided by the soil shear strength.

The factor of safety is a way of describing the stability of a slope and is defined as the ratio between the average shear strength, τ_f, and the corresponding mobilised shear stress, τ_{mob}, along the failure surface (Wu & Kraft, 1970), see equation (2.9). A factor of safety equal to 1,0 represents a limiting equilibrium state in which the slope is on the verge of failure (Sällfors, 2013). Increasing values of the factor of safety indicate larger margin against failure and thus indicate more stable conditions.

$$FoS = \frac{\tau_f}{\tau_{\text{mob}}} \tag{2.9}$$

Classical stability analyses rely according to Alén et al. (2000) on several assumptions. A uniform degree of mobilisation is assumed along the entire failure surface, resulting in a constant factor of safety. The analysis only considers force equilibrium within the sliding mass and does not account for stresses in the surrounding soil. To enable computation, Bishop's method of slices (Bishop, 1954), divides the sliding mass into vertical slices that are analysed individually (Alén et al., 2000). The interaction between slices is simplified using interslice forces. The factor of safety depends on the assumed failure surface, meaning the analysis aims to identify the critical slip surface with the lowest factor of safety. Material parameters are evaluated at the midpoint of each slice and assumed constant within the slice.

According to Skredkommissionen (1995), the required factor of safety depends on factors such as soil conditions, analysis method and consequences of failure. The factor of safety should therefore be interpreted as a relative measure of stability, influenced by uncertainties in soil properties, pore pressure conditions and modelling assumptions. Skredkommissionen (1995) further emphasizes that the required factor of safety depends on the extent and quality of geotechnical investigation. In preliminary stages, conservative soil parameters should be adopted and higher factor of safety achieved. This reflects the greater uncertainties associated with limited investigation basis. In more detailed or advanced investigations, where both undrained and combined analyses are performed and uncertainties are reduced, the required safety levels may be more adjusted and in some cases lower. Furthermore, it should be noted that uncertainties related to load increases and vibrations from ongoing construction activities must be eliminated and that stricter restrictions for future activities are imposed (SGI, 2023). In Figure 2.9, the recommended factors of safety are presented.

Stage	Land use			
	New development	Existing buildings and facilities	Other land	Natural land
Geotechnical inspection and overview calculation	More detailed investigation shall be performed	$F_c > 2$ + $F_{c\phi} > 1.5$	$F_c > 2$ + $F_{c\phi} > 1.5$	F_c, F_{KOMB} and $F_\phi > 1$ (Provided that surrounding land is not affected)
Detailed investigation	$F_c \geq 1{,}7 - 1{,}5$ + $F_{KOMB} \geq 1{,}45 - 1{,}35$ + $F_\phi \geq 1{,}3$ (sand)	$F_c \geq 1{,}7 - 1{,}5$ + $F_{KOMB} \geq 1{,}45 - 1{,}35$ + $F_\phi \geq 1{,}3$ (sand)	$F_c \geq 1{,}6 - 1{,}4$ + $F_{KOMB} \geq 1{,}4 - 1{,}3$ + $F_\phi \geq 1{,}3$ (sand)	F_c, F_{KOMB} and $F_\phi > 1$ (Provided that surrounding land is not affected)
Advanced investigation (and supplementary investigation)	$F_c \geq 1{,}5 - 1{,}4$ + $F_{KOMB} \geq 1{,}35 - 1{,}30$ + $F_\phi \geq 1{,}3$ (sand)	$F_c \geq 1{,}4 - 1{,}3$ + $F_{KOMB} \geq 1{,}30 - 1{,}20$ + $F_\phi \geq 1{,}3 - 1{,}2$ (sand) Under the condition that restrictions are introduced.	$F_c \geq 1{,}3 - 1{,}2^*$ + $F_{KOMB} \geq 1{,}2 - 1{,}15^*$ + $F_\phi \geq 1{,}2 - 1{,}15$ (sand) * Lower values refer to existing facilities of minor importance.	F_c, F_{KOMB} and $F_\phi > 1$ (Provided that surrounding land is not affected)

Figure 2.9: Recommended factors of safety according to Skredkommissionen (1995).

2.8 Combined stability analysis

In combined stability analysis, the shear strength of cohesive soil layers is defined as the minimum of the drained and undrained strengths within each calculation slice along the analysed slip surface (Larsson, 1983). For each lamella in the slip surface, either drained or undrained shear strength parameters are applied, and the lowest applicable shear strength is adopted locally in the stability calculation. This approach allows different parts of the potential failure mechanism to be governed by different drainage conditions which reflects the spatial variability of pore pressure dissipation in soft clays (IEG, 2008).

This concept can also be illustrated by the shear strength envelope shown in Figure 2.10. The shear strength initially follows the drained Mohr–Coulomb criterion, but is limited by the undrained shear strength, c_u. This means that the shear strength will not exceed the undrained shear strength, even if the drained formulation would predict higher values at increasing effective stresses (Seequent, 2022). Consequently, the mobilised shear strength is governed by the minimum of the drained and undrained strengths at any given point along the slip surface.

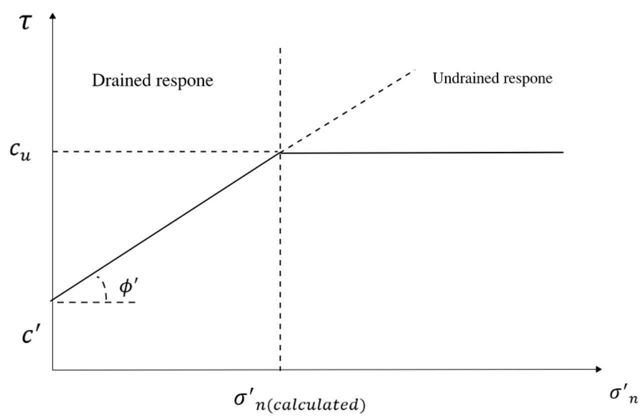

Figure 2.10: Combined frictional-undrained strength model, based on (Seequent, 2025).

The purpose of applying a combined stability analysis in temporary excavations is to obtain a representative estimation of the governing factor of safety for conditions where neither purely undrained nor fully drained assumptions are appropriate. By allowing the shear strength along the potential slip surface to be governed locally by the lowest of the drained and undrained strengths, the combined approach may result in a lower dimensioning factor of safety compared to a purely undrained analysis (SGI, 2023). For contractors involved in infrastructure and foundation projects, understanding when combined stability analysis is appropriate can support design decisions that maintain an adequate level of safety while enabling more cost-efficient solutions for temporary excavation stages.

2.9 Recommended excavation geometries in Swedish practice

The excavation geometries analysed in this study were selected based on the cross sections and recommendations presented in *Schakta säkert* by Lundström et al., 2015. The publication provides guidance regarding temporary excavations and recommended slope inclinations for soil conditions commonly encountered in Swedish practice. For clay excavations, the recommendations are based on specified soil conditions and undrained shear strength levels. The publication presents a set of standardized excavation geometries, referred to type sections, that are intended to serve as practical guidance for safe excavations (Lundström et al., 2015). The type sections cover a range of conditions including varying undrained shear strength of the clay, dry crust thickness and applied surface loading near the slope crest. An example of a type section is shown in Figure 2.11, where the clay is assumed to have a minimum undrained shear strength of c_u=15 kPa, a minimum of 1 m thick dry crust layer and no surcharge load is applied. The recommended slope inclination for these conditions is 1:1 with a maximum excavation depth of 2,75 m. Additional type sections covering a wider range of soil conditions and shear strength levels are presented in Lundström et al. (2015).

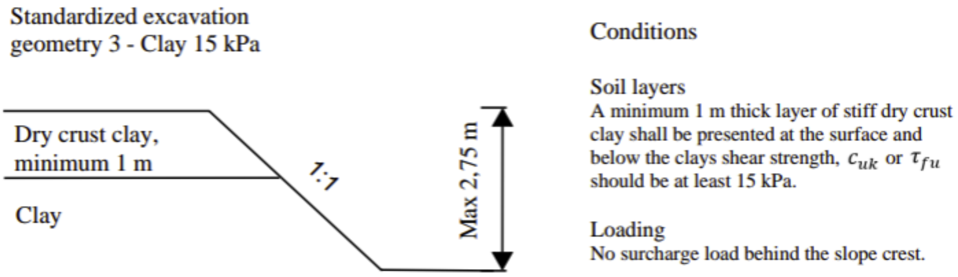

Figure 2.11: Recommended excavation geometry for clay with undrained shear strength of 15 kPa based on (Lundström et al., 2015).

However, it should be noted that the recommendations are presented as guidance and do not explicitly address how the stability of an excavation evolve with time after excavation. The guidance is formulated using undrained shear strength parameters meaning it reflects short-term conditions. The influence of pore pressure dissipation and time-dependent changes in the stability such as reduction in shear strength following excavation are therefore not discussed. No guidance is provided on how long an excavation following a given type section can be assumed to remain stable.

2.10 PLAXIS 2D

PLAXIS 2D is a finite element software developed for geotechnical engineering applications. The program is designed to model and analyse the mechanical behaviour of soil and rock under various loading conditions by using the Finite Element Method. It enables the calculation of deformations, stresses, stability and groundwater flow in geotechnical structures (Bentley Systems, 2025b).

In PLAXIS 2D, geotechnical problems can be idealised as either plane strain or axisymmetric conditions depending on the geometry and loading characteristics, see Figure 2.12. The chosen formulation determines how stress, strains and forces are interpreted in the numerical analysis (Bentley Systems, 2025b). Plane strain formulation is suitable for structures with a uniform cross-section consistent loading over a significant length perpendicular to the analysed section. The model is defined in the x-y plane and strains in the out-of-plane direction are assumed to be zero (ε_{zz}=0), while the corresponding normal stress (σ_{zz}) is included in the calculations. Computed forces therefore represent forces per unit length. Typical applications include slopes, retaining walls and tunnels. Axisymmetric modelling is applied to circular structures exhibiting rotational symmetry around a central axis. In this case, the x-coordinate represents the radial direction and the y-axis corresponds to the axis of symmetry. Stresses and deformations are assumed to be identical in all angular directions. Unlike plane strain, the tangential strain is not zero but is calculated as

$$\varepsilon_{zz} = \frac{u_x}{x} \tag{2.10}$$

where u_x is the radial displacement and x the radial coordinate (Bentley Systems, 2025b). This formulation is appropriate for circular foundations, shafts and similar geometries.

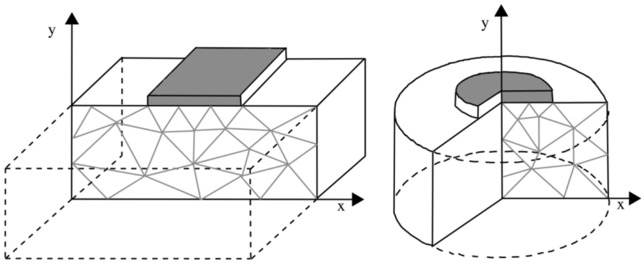

Figure 2.12: Plain strain to the left and axisymmetrical to the right, based on (Bentley Systems, 2025b).

2.10.1 Mohr-Coulomb model

The Mohr-Coulomb model is a linear elastic perfectly plastic constitutive model commonly used as a first approximation of soil and rock behaviour in geotechnical analyses (Bentley Systems, 2025a). It is often recommended for preliminary assessments, as it requires relatively few input parameters, is computationally efficient and provides an initial estimation of deformations and stability.

The Mohr-Coulomb model consists of two main components, elastic and plastic. The elastic behaviour follows Hooke´s law for isotropic elasticity and describes the soil response prior to yielding. Within this range, the stress-strain relationship is linear and fully recoverable upon unloading. Beyond this stress level, deformations are calculated assuming perfect plasticity (Karstunen & Amavasai, 2017). The total strain may therefore be decomposed into an elastic and a plastic component, see Equation 2.11. The material behaves linearly up to the yield stress and beyond that point, plastic strains develop at constant stress which represents a perfectly plastic behaviour, see Figure 2.13.

$$\varepsilon = \varepsilon^e + \varepsilon^p \tag{2.11}$$

The idealised elastic-perfectly plastic stress-strain response described by Equation 2.11 is illustrated schematically in Figure 2.13.

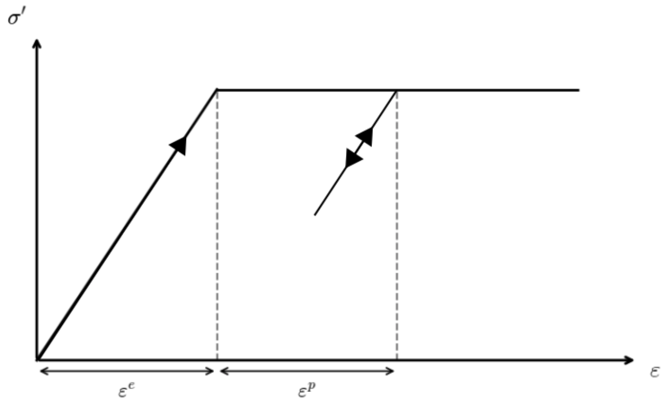

Figure 2.13: Elastic and perfectly plastic model, based on (Bentley Systems, 2025a).

The plastic behaviour is governed by the Mohr-Coulomb failure criterion, see equation 2.12.

$$\tau_f = c' + \sigma' \tan \phi' \tag{2.12}$$

The Mohr-Coulomb failure criterion can be illustrated as shown in Figure 2.14.

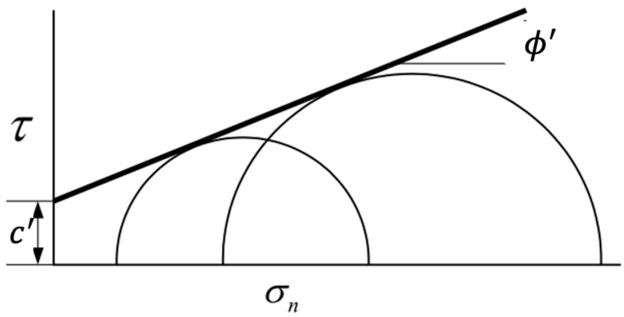

Figure 2.14: Mohr-Coulomb failure criterion for drained conditions, based on (Bentley Systems, 2025a).

where c' is effective cohesion and ϕ' is the friction angle. Yielding occurs when the Mohr circle, defined by the principal stresses σ_1 and σ_3, becomes tangent to the failure envelope (Knappett & Craig, 2012). The Mohr-Coulomb model is defined by five material parameters. Young´s modulus, E, describes the stiffness of the soil within the elastic range, alternatively the shear modulus G, could be used as the stiffness parameter. Poisson´s ratio, ν, defines the relationship between axial and lateral deformations under elastic loading. The dilatancy angle, ψ, governs the volumetric change that occur during plastic shearing and is particularly relevant for dense soils where volume expansion may occur at failure (Bentley Systems, 2025a). According to Hooke's law, the relationship between E, G and ν is given by Equation

2.13 below.

$$G = \frac{E}{2(1+\nu)} \tag{2.13}$$

2.10.2 Drainage type

In PLAXIS the drainage type of a material is defined to control how the program handles pore pressures and soil strength during loading and unloading (Bentley Systems, 2025a). Three commonly used types are Drained, Undrained A and Undrained B. In the Drained analysis, it is assumed that any generated pore pressures dissipate fully, meaning that no excess pore pressures develop. The analysis is performed as an effective stress analysis using the soils effective strength parameters c' and ϕ' (Bentley Systems, 2025a). Drained analysis is the choice for soils with high permeability as well as for long-term analyses where pore pressures are assumed to have fully equalized.

Undrained A is an undrained effective stress analysis in which the soils effective strength parameters (c' and ϕ') and effective stiffness parameters (E' and ν') are used as input (Bentley Systems, 2025a). To model the undrained behaviour, PLAXIS 2D adds the bulk stiffness of water to the stiffness matrix which enables a separate calculation of effective stresses and excess pore pressures. An important limitation of Undrained A is that it may not reproduce the correct undrained shear stress path and potentially yielding an unrealistic undrained shear strength (c_u). It is therefore recommended to set the dilatancy angle to ψ=0 to avoid an unrealistic strength increase caused by tensile pore water pressures (Bentley Systems, 2025a). Undrained B is an undrained effective stress analysis where the undrained shear strength is specified directly by setting ϕ=0 and $c = c_u$ while the stiffness parameters remain effective. This gives a control over c_u regardless of the stress path but a drawback is that the model does not automatically account for the strength gain that occurs during consolidation (Bentley Systems, 2025a).

2.10.3 Safety calculation (phi/c reduction)

Slope stability in PLAXIS 2D is assessed using *Safety* calculation type which is based on the phi/c reduction method. This method progressively reduces the shear strength parameters (ϕ and c) by applying a strength reduction factor until failure is reached (Bentley Systems, 2025b). The reduction is performed according to:

$$\Sigma\mathrm{Msf} = \frac{\tan(\phi_{\mathrm{input}})}{\tan(\phi_{\mathrm{reduced}})} = \frac{c'_{\mathrm{input}}}{c'_{\mathrm{reduced}}} \tag{2.14}$$

At the start of the calculation, ΣM_{sf} is set to 1,0, meaning the full unreduced strength is applied. The multiplier is then incrementally increased until a developed failure mechanism is obtained. Failure is identified when the numerical model can no longer reach equilibrium and the corresponding value of ΣM_{sf} is interpreted as the factor of safety. The strength reduction method yields factors of safety comparable to those from conventional Limit Equilibrium Methods (LEM) such as slip surface analyses (Bentley Systems, 2025b). An advantage is that the critical failure surface is identified automatically without the need to predefine slip surfaces.

2.11 SLOPE/W

SLOPE/W is a slope stability analysis software included in the GeoStudio suite (Seequent, 2025). The program is primarily based on the Limit Equilibrium Method (LEM) which evaluates the stability of slopes by analysing the equilibrium of a potential sliding mass.

2.11.1 General framework and Limit Equilibrium Method

The LEM is based on the assumption that failure occurs along a predefined slip surface, and that the soil mass above this surface behaves as a rigid body at the onset of failure (Seequent, 2025). At limiting equilibrium, the sliding mass is considered to be on the verge of failure such that the governing equilibrium conditions are satisfied.

Various approaches exist within the framework of the LEM for assessing slope stability (Seequent, 2025). These approaches differ primarily with respect to, which equilibrium conditions are satisfied and the assumed relationship between the interslice shear and normal forces are defined (Seequent, 2025). To illustrate the underlying concept a two dimensional potential sliding mass may be subdivided into a number of vertical slices. For each slice a free body diagram can be established. Normal and shear forces act along the base of the slice, while interslice normal and shear forces act along the vertical edges between adjacent slices. The weight of each slice contributes to the overall force system. The factor of safety is defined as the ratio between the available shear strength along the slip surface and the mobilized shear stress required to maintain equilibrium, see Equation (2.9). The assumed slip surface may be circular, composite or fully specified by a series of straight line segments (translational). SLOPE/W searches for the critical slip surface, defined as the surface yielding the lowest factor of safety within the analysed domain.

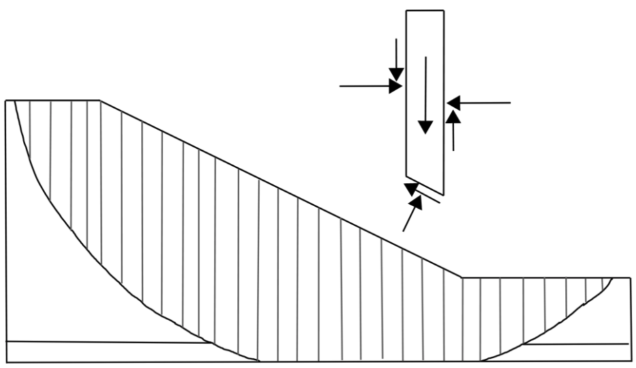

Figure 2.15: Slices and defined forces for a sliding mass, based on (Seequent, 2025).

2.11.2 Slice methods

Within the LEM framework several slice methods are available (Seequent, 2025). These methods differ primarily in terms of how the equilibrium equations are satisfied and in how interslice forces are treated. Simplified methods such as Ordinary method also known as the Fellenius method, neglect all interslice shear forces and satisfy only moment equilibrium in a simplified manner. The Bishop simplified method satisfies overall moment equilibrium but does not fully satisfy horizontal force equilibrium. Similarly the Janbu method satisfies overall force equilibrium but does not fully enforce moment equilibrium.

More rigorous method such as Spencer and Morgenstern-Price satisfy both overall force equilibrium and moment equilibrium simultaneously (Seequent, 2025). These methods account for both interslice normal and shear forces and are formulated within the General Limit Equilibrium (GLE) framework. In the GLE formulation, two factors of safety are calculated: one from force equilibrium and one from moment equilibrium. For methods such as Spencer or Morgenstern-Price, the final factor of safety is obtained at the point where these two conditions are satisfied (Seequent, 2025). The primary difference between the two methods lies in the assumed distribution of interslice shear force. The Spencer method assumes a constant relationship between interslice shear and normal forces along the slip surface whereas the Morgenstern-Price method allows this relationship to vary according to a specified disturbance commonly a half-sin function.

2.11.3 Material models

Different material models can be used in SLOPE/W to represent soil behaviour under various drainage and stress conditions. The choice of material model influences how shear strength is mobilized and how the relationship between pore pressure, effective stress and failure is represented in the stability analysis.

Mohr-Coulomb

In the material model Mohr-Coulomb in SLOPE/W, the soil behaviour is represented based on the Mohr-Coulomb failure criterion. The choice of input parameters determines wheatear the analysis represents drained or undrained conditions (Seequent, 2025). In its standard form, the Mohr-Coulomb model uses effective stress parameters, where the shear strength is defined by the effective cohesion and the effective friction angle, more detailed described in Section 2.3. In this formulation, the pore water pressure is explicitly accounted for through its efficacy in the effective stress. This corresponds to drained conditions, where excess pore pressures have dissipated and the soil response is governed by effective stresses.

The same Mohr-Coulomb model can also be used to represent undrained conditions by modifying the input parameters. In such cases the friction angle is set to zero and the cohesion is defined as the undrained shear strength. This transforms the model into a total stress formulation, where the shear strength is constant and independent of normal stress. Since the analysis is performed in terms of total stress, pore water pressure does not influence the calculated shear strength.

Combined stability analysis

The Combined model in SLOPE/W can be used to represent both drained and undrained shear strength conditions. A detailed description of the combined analysis approach is provided in Section 2.8. In SLOPE/W, the model evaluates both the drained Mohr-Coulomb strength and the undrained shear strength and adopts the lower value. Both the effective cohesion and the undrained shear strength can be defined as depth-dependent parameters through specified gradients or by defining a c'/c_u ratio, from which c' is calculated (Seequent, 2022).

Shear-Normal Function

The Shear-Normal Function (SNF) model defines shear strength as a direct relationship between shear stress, τ, and effective normal stress, σ'_n, rather than through constant Mohr-Coulomb parameters. The failure envelope is specified using a series of discrete σ'_n, τ data points that form a non-linear shear strength function (Seequent, n.d.).

During the stability analysis, SLOPE/W evaluates the effective normal stress at the base of each slice and identifies the corresponding point on the shear-normal curve. Then a tangent is fitted to the curve at that stress level. The slope of the tangent defines an equivalent friction angle, while the intercept with the shear stress axis defines an equivalent cohesion, as illustrated in Figure 2.16. These equivalent parameters are used internally by SLOPE/W to calculate the shear resistance of each slice. The SNF model allows the shear strength to vary with effective normal stress and can therefore represent non-linear soil behaviour that cannot be captured by a conventional Mohr-Coulomb model with constant strength parameters (Seequent, n.d.).

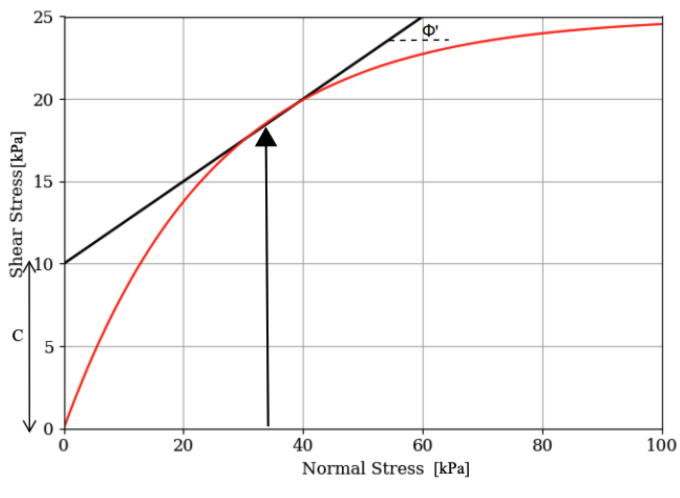

Figure 2.16: Representation of c' and ϕ' from a non-linear failure envelope, based on (Seequent, n.d.).

Consequently c' and ϕ' are stress-dependent and vary along the slip surface as functions of the local effective normal stress. In regions where the shear-normal relationship is approximately linear, the derived parameters remain nearly constant, whereas more curvature leads to variation in the mobilized values between slices.

2.11.4 Pore water pressure conditions

In SLOPE/W pore water pressure conditions can be defined using several methods depending on the complexity of the problem and the available data. Since pore water pressure directly influence the effective stress it plays an important role in determining the shear strength and the stability of a slope.

Piezometric surface

The Piezometric surface method is a way to define the pore water pressure condition in SLOPE/W (Seequent, 2025). It represents the level to which water would rise in a piezometer and is used to approximate groundwater conditions. The surface is defined either by drawing a line or by specifying coordinates within the model domain. In this method the pore water pressure at the base of each slice is calculated from the vertical distance between the slice base and piezometric surface multiplied by the unit weight of water. This results in a hydrostatic pore pressure distribution. This implies that the pore water pressure is assumed to increase linearly with depth. If the slice base is located above the piezometric surface, negative pore water pressure will occur but will not be included as a contribution to shear strength unless it is explicitly defined in the analysis, see chapter 2.11.4 (Seequent, 2025).

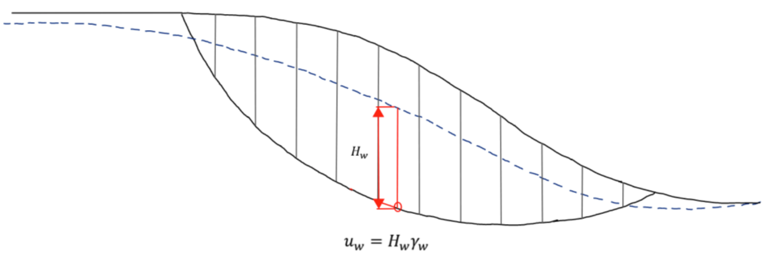

Figure 2.17: Pore water pressure from a piezometric surface, based on (Seequent, 2025)

Spatial function

The Spatial function is a method that can be used to define the pressure conditions of the pore water by assigning the pressure head values at discrete points within the model domain (Seequent, 2025). These values can be defined manually or imported from external sources, such as numerical analyses or field measurements. The pressure head represent the equivalent height of a water column and is related to the pore water pressure according to:

$$h = \frac{u}{\gamma_w} \tag{2.15}$$

where h is the pressure head in meter, u is the pore water pressure in $\mathrm{kN/m^2}$, and γ_w is the unit weight of water. The unit weight of water is assumed to be $\gamma_w = 9,81\,\mathrm{kN/m^3}$.

From the spatial function defined by discrete data points, the solver generates a continuous pore water pressure distribution over the model domain using interpolation techniques (Seequent, 2025). In SLOPE/W this is done using either krigged or linear interpolation. Krigged interpolation generates a continuous pore water pressure distribution by estimating values between data points based on their spatial relationship. The method considers both the distance and variation between points to construct a smooth surface that passes through the defined values. Linear interpolation determines values between data points by connecting them with straight lines. The pore water pressure is calculated directly between nearby points without considering any additional spatial variation.

Inclusion of negative pore water pressure in SLOPE/W

In SLOPE/W, negative pore pressure can contribute to increased shear strength if an unsaturated formulation is adopted (Seequent, 2025). Above the groundwater table the pore water pressure is negative which is commonly refered to as matric suction. The shear strength is expressed using an extended Mohr-Coulomb criterion, see 2.5. If no unsaturated formulation is defined, negative pore water pressure do not contribute to shear strength and therefore do not directly influence the factor of safety (Seequent, 2025).

The additional suction strength term in the extended Mohr-Coulomb equation is governed by the angle ϕ^b, which defines how efficiently matric suction increases shear strength. In the saturated capillary zone immediately above the groundwater table ϕ^b equals to ϕ', meaning that suction is as effective at mobilising shear strength as positive effective stress. As the degree of saturation decreases further above the water table, ϕ^b decreases accordingly. In practice ϕ^b=1/2 ϕ' is a common estimate, with typical values ranging from 15-20 degrees (Seequent, 2022). Setting ϕ^b to zero in the model conditions means ignoring any suction contribution.

2.11.5 Identification of the critical slip surface

The identification of the critical slip surface in SLOPE/W is carried out through a trial procedure (Seequent, 2025). A potential slip surface is generated and the corresponding factor of safety is calculated. This process is repeated for a large number of possible slip surface and the surface yielding the lowest factor of safety is defined as the critical slip surface. Several approaches are available for defining the geometry and position of trial slip surface.

Grid and Radius

The Grid and Radius method is commonly used to generate circular trial slip surfaces (Seequent, 2025). In this method, a grid of potential circle centers is defined above or around the slope. For each grid point, a range of possible radius is specified, thereby creating multiple circular arcs that intersect the slope. Each combination of a grid center and a radius defines a circular trial slip surface. The portion of the circle located below the ground surface defines the potential sliding mass. The factor of safety is then calculated for each generated surface. This approach enables a systematic and extensive search for circular failure mechanisms. However, the search is constrained by the predefined grid density and radius range. A coarse grid may overlook the global minimum, whereas an overly refined grid increases computational effort.

Entry and Exit

The Entry and Exit method provides a more controlled approach for defining circular trial slip surfaces (Seequent, 2025). Instead of prescribing circle centres, entry and exit zones are defined along the ground surface. Points within the entry zone are paired with points in the exit zone, and circular arcs are generated through these locations. This method allow to visualize and restrict the potential failure region prior to performing the calculation. By adjusting the location of the entry and exit zones, different failure mechanisms can be isolated and examined separately. Additional geometric constraints are imposed to prevent unrealistic slip surfaces, such as excessively flat circles or undercutting geometries. The generated circular surfaces are subsequently analysed in the same manner as in the Grid and Radius method.

3 Methods

The methodology used in this thesis consisted of three main parts. In the first part, finite element analyses were performed in PLAXIS 2D to simulate the excavation process and the subsequent time-dependent pore pressure dissipation in clay. Different excavation geometries and consolidation phases were analysed in order to evaluate how pore water pressures and effective stresses evolve with time after excavation.

In the second part, the pore water pressure distributions obtained from PLAXIS 2D were exported and implemented in SLOPE/W where slope stability analyses were performed using the limit equilibrium method. This combined approach enabled the temporal development of the factor of safety to be evaluated while accounting for the changing pore pressure conditions during consolidation.

In the final part, a sensitivity analysis was carried out to investigate how variations in material parameters influence the stability behaviour and the temporal development of the factor of safety. The sensitivity analyses were performed by varying one parameter at a time while keeping all other parameters constant.

3.1 Numerical modelling

The numerical analyses were carried out using a combined approach, where the finite element method (FEM) was used to simulate stress and pore water pressure conditions and the limit equilibrium method was used to evaluate the slope stability. The FEM analyses were performed in PLAXIS 2D and the LEM analyses were performed in SLOPE/W. All models were constructed using the same geometry, material properties and groundwater conditions in both programs.

Three excavation geometries were analysed. The primary geometry, based on recommendations from Schakta Säkert, (Lundström et al., 2015), consists of an excavation depth of 2,75 m and a slope inclination of 1:1, as illustrated in Figure 3.1. In addition, two alternative geometries with the same excavation depth were analysed, with slope inclinations of 1:1,5 and 1:2 respectively, as shown in Figure 3.2. The soil profile consists of two layers, an upper layer of fill material with a thickness of 1 m, representing a dry crust, and an underlying homogeneous clay layer of 19 m. The width of the three geometry models is 19 m, while the length of the excavation bottom was selected as 2 m. The groundwater table was set at 1 m below the ground surface, coinciding with the interface between the fill material and the clay layer.

All models were defined using the same material parameters and groundwater conditions. However, as some parameters are defined differently between PLAXIS 2D and SLOPE/W, the adopted parameters are presented separately for each program in Tables 3.2 and 3.4 in the following sections.

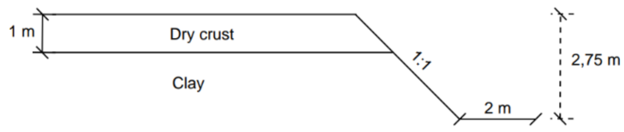

Figure 3.1: Geometry of the excavation with a slope inclination of 1:1.

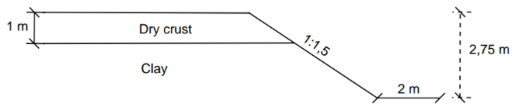

(a) Slope inclination 1:1,5

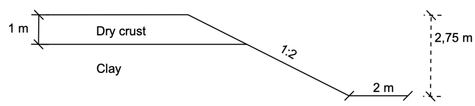

(b) Slope inclination 1:2

Figure 3.2: Geometry of two excavations with slope inclinations of 1:1,5 and 1:2

3.1.1 PLAXIS 2D

The analyses in PLAXIS 2D were conducted under the assumptions of plane strain conditions, implying that the geometry and loading are constant in the out-of-plane direction. This assumption is appropriate for slope stability problems where the geometry can be considered uniform along its length. The model was discretised using 15-noded triangular elements and the mesh density was chosen to ensure sufficient refinement in critical areas, particularly around the slope and excavation bottom. A mesh sensitivity analysis was performed to evaluate the influence of mesh refinement on the calculated factors of safety. As shown in Table 3.1, three different mesh densities were tested and the resulting factors of safety were compared for selected time steps. The results show only minor differences between the medium and fine meshes, indicating that further mesh refinement has a negligible influence on the stability results. Based on this assessment, the medium mesh was considered sufficiently refined for the analyses. Particular attention was given to maintaining a finer mesh around the excavation slope and beneath the excavation base, where the largest pore pressure gradients occur. This was important to provide an adequate number of data points for the pore pressure transfer to SLOPE/W, minimising the need for interpolation in the critical zones where pore pressure gradients are steep. The final mesh for the model is shown in Figure 3.3. The mesh sensitivity analysis was performed only for the 1:1 slope geometry, and the resulting mesh was subsequently adopted for the 1:1,5 and 1:2 slopes. The meshes used for the remaining slope geometries are presented in Appendix A.

Table 3.1: Mesh sensitivity analysis, where FoS values were obtained from the SLOPE/W stability analyses for slope 1:1.

Element	Nodes	FoS 1day	FoS 25days	FoS 50days
654	5337	1,250	1,168	1,114
1643	13335	1,260	1,179	1,126
2179	17655	1,260	1,179	1,126

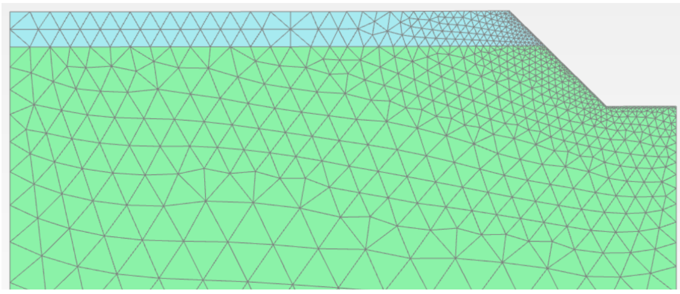

Figure 3.3: Final mesh in PLAXIS 2D for the slope inclination 1:1.

Two different materials were defined in the model. The fill material was modelled using Mohr-Coulomb with drainage type Drained, reflecting its relatively high permeability and ability to dissipate pore pressure rapidly. The clay layer was also modelled using Mohr-Coulomb but with the drainage type set to Undrained A. This approach allows the use of effective stress parameters while simulating undrained behaviour through the generation of negative excess pore pressure, which is suitable for short-term conditions immediately following excavation. The adopted material parameters are presented in Table 3.2 below.

Table 3.2: Material parameters used in the PLAXIS 2D analysis.

Parameter	Unit	Fill layer	Clay layer
γ	kN/m^3	18	17
ν	–	0,2	0,2
c'	kPa	3	1,5
ϕ'	$^\circ$	30	30
c_u	kPa	30	15
k_x	m/s	$1{,}16 \times 10^{-8}$	$1,04 \times 10^{-9}$
k_y	m/s	$1{,}16 \times 10^{-8}$	$1,04 \times 10^{-9}$
E'_{ref}	kN/m^2	10800	4050
G_{ref}	kN/m^2	4500	1688
E_{oed}	kN/m^2	12000	4500

Boundary conditions were defined for both hydraulic and mechanical behaviour. For the hydraulic conditions, the upper and lower boundaries were set as open, allowing pore water flow, while the vertical boundaries were defined as closed to simulate symmetry and preventing lateral groundwater flow. Mechanically, the vertical boundaries (x-min and x-max) were set to normally fixed, restricting horizontal displacements. The bottom boundary (y-min) was fully fixed and the ground surface (y-max) was left free.

In order to avoid sharp changes in pore pressure the slope surface and excavation bottom, a thin drainage layer with a thickness of 1 cm was created along the excavated slope and bottom. This was done by allowing that cluster to interpolate with the pore pressures nearby. The purpose of this modelling approach was to allow drainage along the slope surface and excavation bottom to capture the suction effects. Furthermore, it prevented the imported pore pressure field in SLOPE/W from being interpreted as a small amount of water in the excavation, and thereby ensuring a consistent pore pressure distribution across the slope and excavation interface. The analysis was carried out in a series of phases to simulate the excavation process and the time-dependent behaviour of the soil. An overview of the phases and their corresponding calculation procedures is shown in Table 3.3. After the initial stress generation and excavation phase, consolidation analyses was performed to model the dissipation of excess pore water pressure over time. Safety analyses (ϕ/c reduction) were then conducted at each time step to follow the factor of safety at each time step. The time parameter t in Phase 4 of Table 3.3 represents the different consolidation time steps analysed throughout the study for each geometry. The full list of time steps included in the analyses is presented in Appendix B. Finally, an additional consolidation phase with Linear Elastic material model was run to determine the fully drained end state, defined as the condition where all excess pore pressures had dissipated.

For each consolidation phase, the pore water pressure values at all nodes in the finite element model were extracted together with their corresponding spatial coordinates. This was repeated for every analysed time step, resulting in a series of nodal pore pressure distribution representing different stages of consolidation following excavation. The extracted data was subsequently exported into SLOPE/W which is describes in detail in the chapter below.

Phase	Description	Type of procedure	Loading type	Time [days]
Initial phase	Soil activation and calculation of initial stresses	K_0-procedure	Staged construction	-
Phase 1	Excavation phase (dry excavation)	Consolidation	Staged construction	1
Phase 2	Consolidation	Consolidation	Staged construction	1
Phase 3	Phi/c reduction (safety analysis)	Safety	Incremental multiplier	-
Phase 4	Consolidation	Consolidation	Staged construction	t
Phase 5	Phi/c reduction (safety analysis)	Safety	Incremental multiplier	-
Phase 6	Fully drained analysis	Consolidation	Minimum excess pore pressure	-

Table 3.3: Description of calculation phases in PLAXIS 2D.

3.1.2 SLOPE/W

The stability analyses were performed in SLOPE/W using the Limit Equilibrium method. The Morgenstern-Price method was selected as it satisfied both force and moment equilibrium which provides a robust calculation of the factor of safety for slopes with complex pore pressure conditions.

The slope geometry was constructed in SLOPE/W to match the geometries described in Section 3.1. The top layer was defined using Mohr-Coloumb material model with drained conditions. For the clay, two separate material models were defined to enable comparison between different analysis conditions: one combined stability model where the shear strength was defined as a function of depth, *S=f(depth)*, and one model using the Shear-Normal Function. For the Shear-Normal function model, the shear strength envelope was defined using data points entered through the shear/normal stress data point function in SLOPE/W. The envelope was constructed by taking the minimum shear strength value of the drained and undrained conditions at each normal stress level. The drained shear strength was defined using the Mohr-Coulomb failure criterion with effective cohesion c' and effective friction angle ϕ', while the undrained shear strength was defined by c_u. As illustrated in Figure 3.4, the resulting envelope transitions between the undrained and drained strength depending on the governing condition. To account for the contribution of negative pore water pressure to shear strength, the suction function must be included in the model. This function is available for the Mohr-Coulomb and Shear-normal function material model, but not for the Combined model. As previously mentioned ϕ_b is set to half of the ϕ' for both the fill and clay layers.

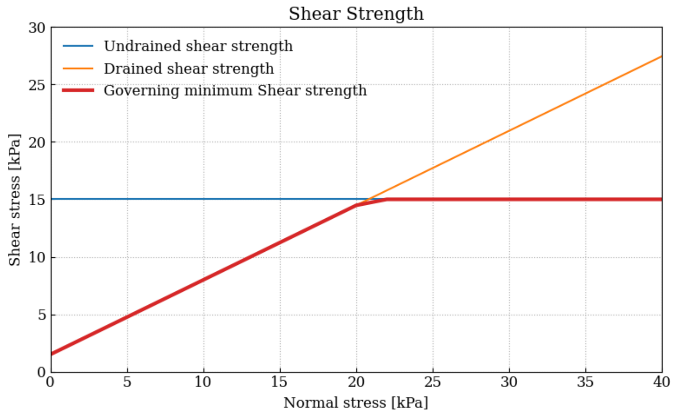

Figure 3.4: Governing shear strength for the Shear-Normal function in SLOPE/W.

The material parameters used in the SLOPE/W analyses are summarized in 3.2.

Table 3.4: Material parameters used in the SLOPE/W analysis

Parameter	Unit	Fill layer	Clay layer
γ	kN/m^3	18	17
c'	kPa	3	1,5
ϕ'	$\circ$	30	30
ϕ^b	$\circ$	15	15
c_u	kPa	–	15
c'/c_u	–	–	0,1

To establish a baseline, three initial analyses were performed where the groundwater conditions were defined manually using the piezometric surface method. The piezometric line was drawn 1 m below the ground surface, following the slope geometry and excavation bottom, representing an upper bound assumption of the groundwater conditions. One analysis was carried out using undrained analysis, one using drained analysis, and one using combined analysis. These served as a baseline for comparison with the analyses that follow.

To investigate how the factor of safety evolves over time, pore pressures obtained from PLAXIS 2D were implemented in SLOPE/W. This was done using Spatial function for the pore water pressure conditions. The pore water pressure data from PLAXIS 2D consist of nodal coordinates and corresponding pore pressure values. Since SLOPE/W requires pressure head as input, the pore pressure was converted according to 2.15. Linear interpolation was used to generate the pore water pressure distribution, determining values between data points by connecting them with straight lines without considering additional spatial variation.

For each analysed time step from PLAXIS 2D, representing different stages of consolidation after excavation, a new spatial function was defined in SLOPE/W. This allowed a separate stability analysis to be performed for each time step, where only the pore pressure distribution varied while all other model parameters remain unchanged.

The search for the critical slip surface for each analysis was performed using the Entry and Exit method. This method constrains the search to predefined surfaces and ensures consistent comparison between analyses, allowing changes in the factor of safety to be attributed primarily to variations in pore pressure.

3.1.3 Sensitivity analysis

To evaluate the influence of individual parameters on the stability results, a sensitivity analysis was performed. The purpose of this analysis was to identify which parameters have the greatest impact on the slope stability and the factor of safety and to quantify the degree to which variations in input parameters affect the results.

The sensitivity analysis was carried out by varying one parameter at a time while keeping all the other parameters constant at their reference values. For some parameters the values were both increased and decreased, and for some only increased. The parameters that were tested and how they were varied is described in Table 3.5 below.

Table 3.5: Parameters tested in the sensitivity analysis and their variations.

Material	Parameter	Symbol	Reference value	Tested values
Clay	Effective cohesion	c'	1,5 kPa	1,2 / 2,0 kPa
Clay	Undrained shear strength	c_u	15 kPa	12 / 20 kPa
Clay	Oedometer modulus	E_{oed}	4500 kPa	7500 / 15000 kPa
Clay	Permeability	k	$1,04 \times 10^{-9}$ m/s	$1,04 \times 10^{-8}$ / $1,04 \times 10^{-7}$ m/s
Clay	Friction angle	ϕ'	30°	27 / 33°
Fill	Effective cohesion	c'	3 kPa	2,4 / 3 kPa
Fill	Undrained shear strength	c_u	30 kPa	–
Fill	Oedometer modulus	E_{oed}	6000 kPa	9000 / 16500 kPa
Fill	Permeability	k	1×10^{-8} m/s	–
Fill	Friction angle	ϕ'	30°	–

For each parameter variation, the analysis was first performed in PLAXIS 2D to obtain the corresponding pore water pressure distribution for all consolidation phases. The resulting nodal pore pressure data was subsequently exported to SLOPE/W, where combined stability analysis was performed for each time step following the same procedure described in 3.1.2. This allowed the effect of each parameter variation to be evaluated in terms of the temporal development of the factor of safety.

For the sensitivity analyses of effective cohesion and oedometer modulus, the corresponding parameters of the fill layer were also adjusted. This was done to maintain a consistent relative stiffness and strength contrast between the filling and the underlying clay throughout the analyses. However, for the effective cohesion of the filling, the tested values did not follow the same proportional variation as for the clay, since the effective cohesion of dry crust is commonly assumed to lie within a relatively limited range of approximately 2–3 kPa (Trafikverket, 2011). For the remaining parameter variations, the filling layer properties were kept at their reference values.

4
Results

In this chapter the main findings from the study are presented. The results include the pore pressure development over time for different excavation and slope geometries, a comparison between pore pressure distribution obtained from PLAXIS 2D and those implemented in SLOPE/W and an investigation of how the suction friction angle ϕ^b influences short-term stability. Furthermore, the gradual transition from undrained to drained conditions is presented in terms of time and the dimensionless time factor, for all analysed slope geometries. Additionally, the distribution of shear strength along the critical slip surface is evaluated at different time stages, providing insight into where along the failure surface the reduction in stability is most pronounced over time. Finally, the results from the sensitivity analysis are presented, examining the influence of individual parameters on the temporal development of the factor of safety.

4.1 Time-dependent pore pressure dissipation following excavation

Figure 4.1 presents the pore pressure distribution obtained in PLAXIS 2D and the corresponding pore pressure distribution implemented in SLOPE/W, for this case directly after excavation. It can be seen that the overall pore pressure distribution patterns are similar between the two models, with both showing negative pore pressures concentrated near the excavation slope surface and increasing pore pressures with depth. For the pore pressure results in PLAXIS 2D, the positive values shown in the legend represent negative pore pressures, as indicated in the Figure 4.1. The distributions indicate that the imported pore pressure conditions in SLOPE/W reasonably reproduce the results obtained from the Finite Element analysis in PLAXIS 2D. It should be noted that the time intervals presented for each geometry are not uniform. The selected time steps represent the stage at which the factor of safety curve begins to converge towards fully drained conditions, after which only negligible changes occur before fully drained conditions are reached. Time steps beyond this point were therefore considered to provide no additional information of significance and have been excluded from the analysis. The complete development of the pore pressure distribution can be found in Appendix C.

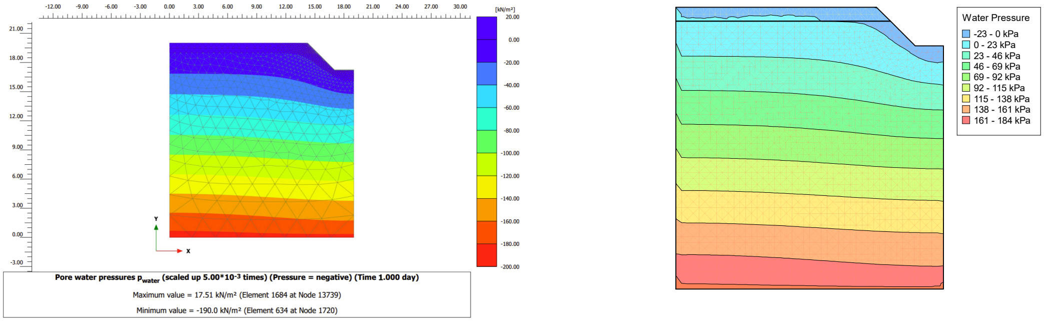

(a) PLAXIS 2D **(b)** SLOPE/W

Figure 4.1: Comparison of pore pressure distributions.

Figure 4.2 illustrates the development of pore pressure distribution over time for a slope with inclination 1:1 and with geometry as illustrated in Figure 3.1. At 1 day after excavation negative pore pressure distribution appear near the slope surface and the bottom of the excavation (blue colours), with the largest suction under the excavation bottom. At 25 days, negative pore pressures are still present, although their magnitude has decreased significantly. At 50 days, the extent of the negative pore pressure zone has decreased and the pore pressure contours have become smoother. At 150 days, the negative pore pressures near the slope surface are further reduced and the pore pressure distribution appears more uniform throughout the slope.

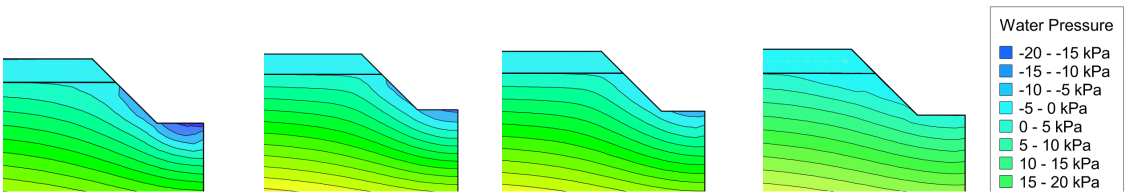

(a) 1 day **(b)** 25 days **(c)** 50 days **(d)** 150 days

Figure 4.2: Development of pore pressure distribution for a slope with inclination 1:1 in SLOPE/W over time.

Figure 4.3 presents the development of pore pressure distribution over time for a slope inclination of 1:1,5. Similar to the 1:1 slope shown in Figure 4.2, negative pore pressures are visible near the slope surface and under the excavation bottom shortly after excavation. However, compared to the steeper 1:1 slope, the negative pore pressure zone extends further into the central part of the slope at 1 day after excavation. At 50 days, the extent of the negative pore pressure zone has decreased considerably, although negative pore pressures are still visible near the slope surface. Compared to the 1:1 slope, traces of negative pore pressures remain visible for a longer period of time, as they can still be observed near the crest and slope surface at 300 days. The pore pressure contours also become more uniform and more stable with increasing time.

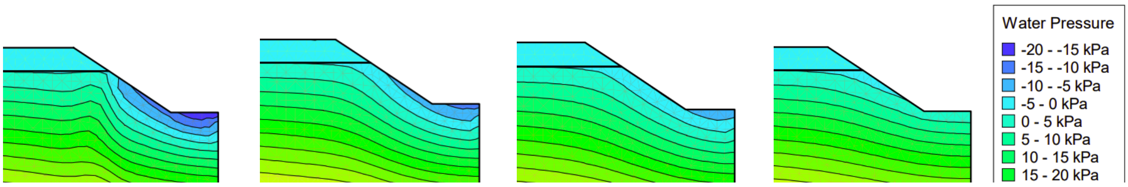

(a) 1 day **(b)** 25 days **(c)** 50 days **(d)** 300 days

Figure 4.3: Development of pore pressure distribution for a slope with inclination 1:1,5 in SLOPE/W over time.

Figure 4.4 illustrates the development of pore pressure distribution over time for a slope with inclination 1:2 and the geometry as shown in 3.2 in SLOPE/W. At 1 day after excavation, lower pore pressures are visible near the slope surface and at the excavation base. Compared to the other slopes, it is clearly seen that this one has the highest proportion of suction and that it extends the most along the slope. At 100 days, the low pore pressure zone has decreased and the pore pressure contours appear smoother throughout the slope. At 500 days, the pore pressure distribution is more uniform, with only small areas of lower pore pressure remaining near the slope surface. Compared to the steeper slopes shown in Figures 4.2 and 4.3, the negative pore pressures persist for a longer period of time, reflecting the more gradual dissipation associated with the flatter slope inclination.

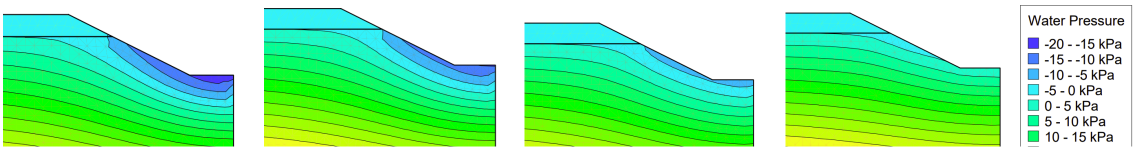

(a) 1 day **(b)** 25 days **(c)** 100 days **(d)** 500 days

Figure 4.4: Development of pore pressure distribution for a slope with inclination 1:2 in SLOPE/W over time.

Figure 4.5 presents the pore pressure at Point P, located in the passive zone of the slip surface, as a function of time after excavation for three excavation geometries. Immediately after excavation, all curves exhibit a sharp drop from hydrostatic pore pressure to approximately -5 to -10 kPa, reflecting the undrained stress relief induced by the excavation. With time, the negative excess pore pressures dissipate and the pore pressure increases gradually towards positive long-term drained values in the range of 3-6 kPa, at a rate that varies with slope inclination, where steeper slopes reach drained conditions more rapidly than flatter ones.

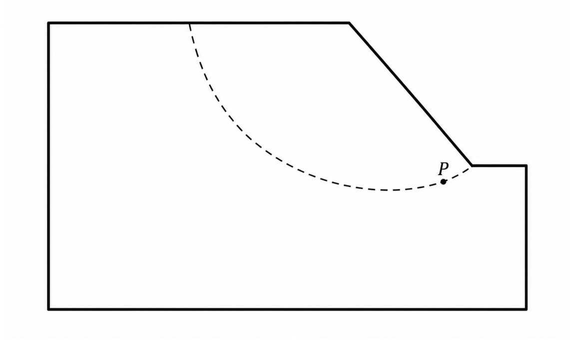

(a) Illustration of point P (passive zone) in the slip surface.

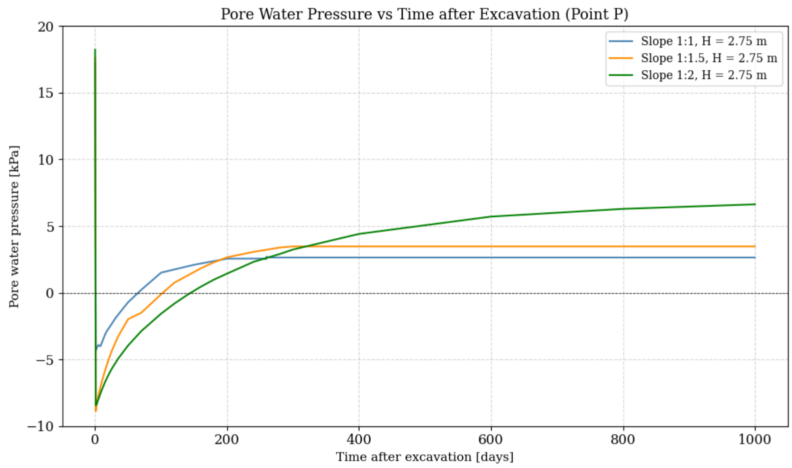

(b) Pore pressure distribution vs time after excavation in the passive zone for a slip surface.

Figure 4.5: Pore pressure distribution in the passive zone in the slip surface.

4.2 Influence of negative pore pressure, ϕ^b

Figure 4.6 presents the variation of FoS with time after excavation for the slope inclination of 1:1 and excavation depth of 2,75m. Three curves are modeled using the material model Shear-Normal Function in SLOPE, with the Mohr-Coloumb shear strength criterion, for $\phi^b = 0°$, 15°, and 30°, respectively. A fourth curve represents the case when the material model *Combined,S=f(depth)*, in SLOPE/W is used.

For the 1:1 slope with an excavation depth of 2,75 m, the initial FoS at $t = 0$ days increases with ϕ^b, ranging from 1,21 for $\phi^b = 0°$ to 1,32 for $\phi^b = 30°$. Initially, the curves exhibit a clear separation, reflecting the contribution of negative pore pressure (suction) to shear strength in the early stages following excavation. As pore pressure dissipate with time, the additional strength provided by suction diminishes, and the curves converge towards a common value. At approximately $t = 70$ days, the curves coincide, indicating that the strength from suction contribution has dissipated entirely by this point. Beyond $t = 70$ days, all cases yield almost the same equivalent FoS, reaching a common long-term value at approximately 1,05.

This behaviour confirms that ϕ^b governs short-term stability, with no influence on the long-term drained conditions. The *Combined,S=f(depth)*, overlaps entirely with the $\phi^b = 0°$ curve throughout the entire consolidation period, suggesting that the combined analysis does not account for any suction contribution from negative pore pressures in the model.

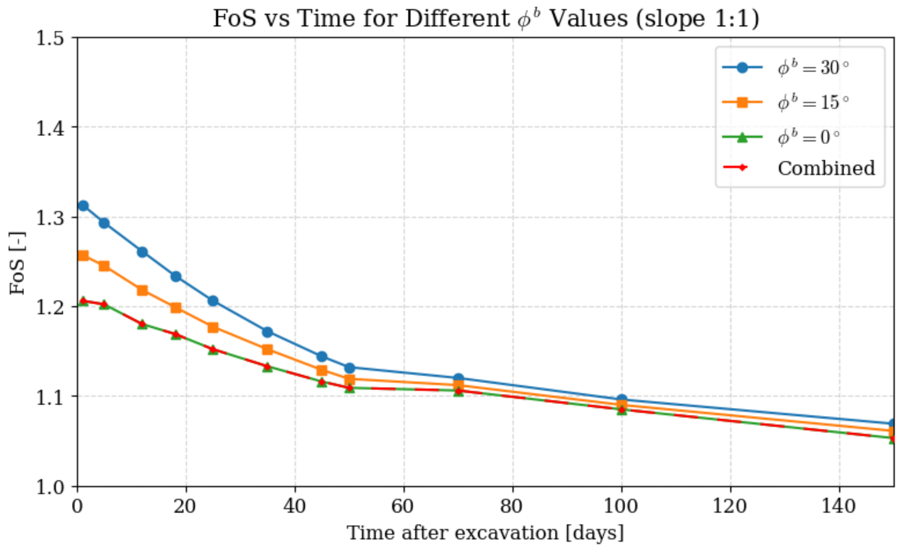

Figure 4.6: FoS with time after excavation for different ϕ^b for a slope inclination of 1:1 and excavation depth 2,75 m

For the 1:1,5 slope with an excavation depth of 2,75 m, the influence of ϕ^b on the initial FoS is slightly more pronounced than for the 1:1 case, with values ranging from 1,35 for $\phi^b = 0°$ to 1,53 for $\phi^b = 30°$ at $t = 0$ days. As with the 1:1 slope, the curves exhibit a clear initial separation that diminishes as pore pressure dissipate over time. The curves converge together as around $t = 100$ days, somewhat later than observed for the steeper slope. Beyond this point, all cases yield an equivalent FoS, reaching a common long-term value of approximately 1,13. This further confirms that ϕ^b only influences short-term stability. As observed for the 1:1 slope, the combined analysis, *Combined,S=f(depth)*, overlaps entirely with the $\phi^b = 0°$ curve, which further supports that the material model does not incorporate any suction contribution from negative pore pressures.

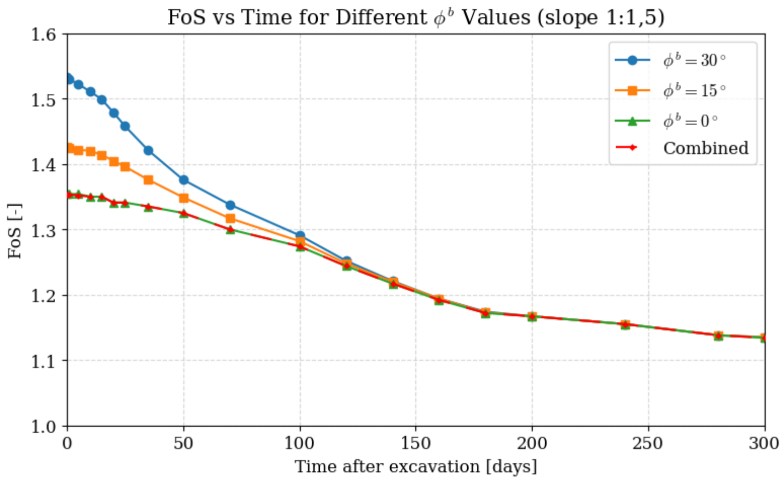

Figure 4.7: FoS with time after excavation for different ϕ^b for a slope inclination of 1:1,5 and excavation depth 2.75 m

Figure 4.8 presents the variation of FoS with time after excavation for slope inclination 1:2 and excavation depth 2,75 m. The initial FoS at $t = 0$ days increase with ϕ^b, ranging from 1,62 for $\phi^b = 0°$ to 1,79 for $\phi^b = 30°$, reflecting the contribution of negative pore pressure to shear strength immediately after excavation. As pore pressure dissipate over time, the curves converge and the separation between diminishes, with all curves reaching approximately the same FoS at $t = 200$ days. As observed for the other slope geometries, the combined analysis overlaps entirely with the $\phi^b = 0°$. Compared with slope 1:1 and 1:1,5, the 1:2 slope exhibit slower transitions to drained conditions.

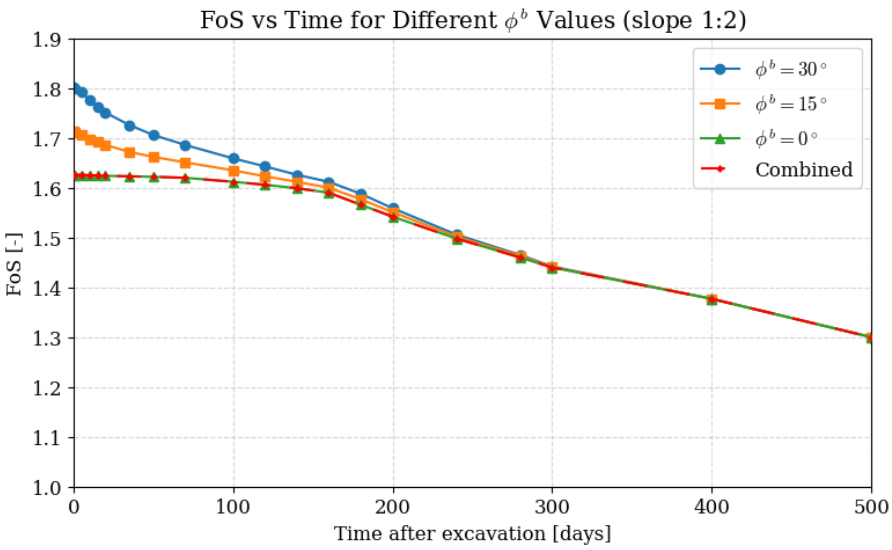

Figure 4.8: FoS with time after excavation for different ϕ^b for a slope inclination of 1:2 and excavation depth 2.75 m

4.3 Shear resistance along critical slip surface

The shear resistance was evaluated along the same slip surface for all time steps for the different slope geometries. The selected slip surface corresponds to the critical slip surface identified at 1 day after excavation as well as the last day identified. The x-axis represents the distance along the slip surface, describing the position along the failure surface through the slope geometry.

For the 1:1 slope shown in Figures 4.10 and 4.9, the critical slip surfaces identified at 1 day and 150 days after excavation are relatively similar in shape and depth. The shear resistance initially increases along the slip surface before reaching a maximum and then decreases towards the toe of the slope. With increasing time after excavation, the shear resistance gradually decreases along most of the slip surface, particularly near the passive zone close to the slope toe where the largest differences between the time steps are observed. In contrast, the active zone near the slope crest is less affected by time-dependent changes.

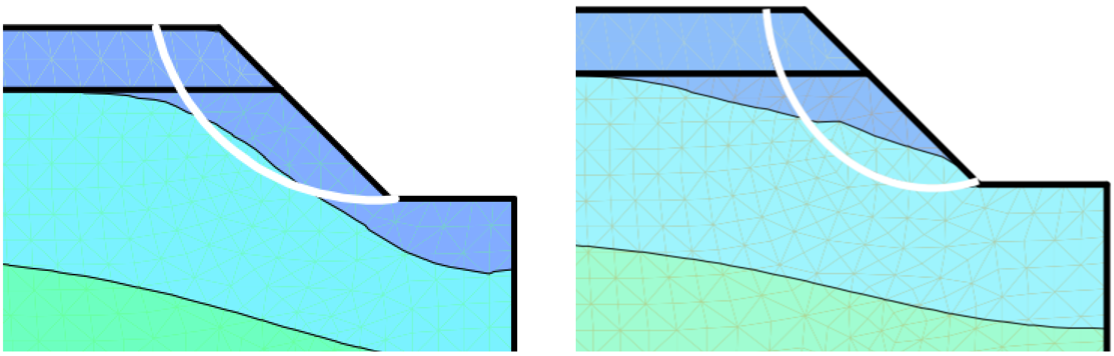

(a) Critical slip surface identified at 1 day after excavation.

(b) Critical slip surface identified at 150 days after excavation.

Figure 4.9: Critical slip surfaces corresponding to the shear resistance distributions shown in Figure 4.10.

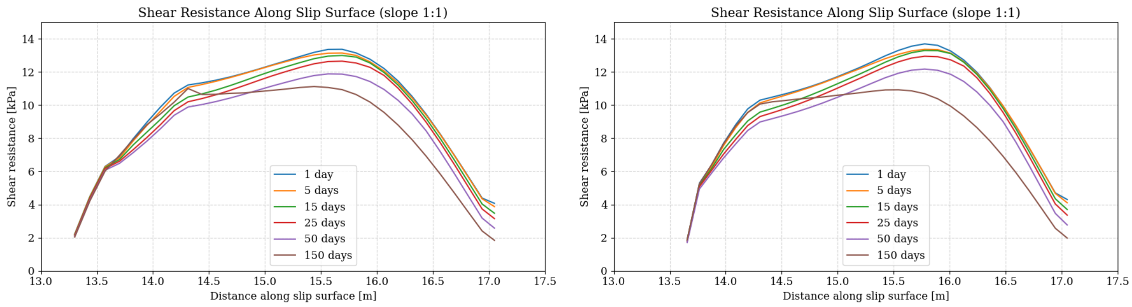

(a) The shear resistance along the slip surface corresponds to the critical slip surface identified 1 day after excavation.

(b) The shear resistance along the slip surface corresponds to the critical slip surface identified 150 days after excavation.

Figure 4.10: Shear resistance along the same slip surface for different times after excavation for slope 1:1.

A similar behaviour can be observed for the 1:1,5 slope in Figures 4.11 and 4.12. The critical slip surfaces identified at 1 day and 300 days after excavation remain relatively similar, and the overall distribution of shear resistance follows the same general trend as for the steeper slope. The shear resistance decreases progressively with time, again with the largest reduction occurring near the toe region. However, for this geometry, a local reduction in shear resistance is visible at approximately x=14 m during the early time steps. This local decrease is likely associated with the groundwater table located 1 m below the ground surface, where pore pressure redistribution following excavation temporarily influences the effective stresses along the slip surface.

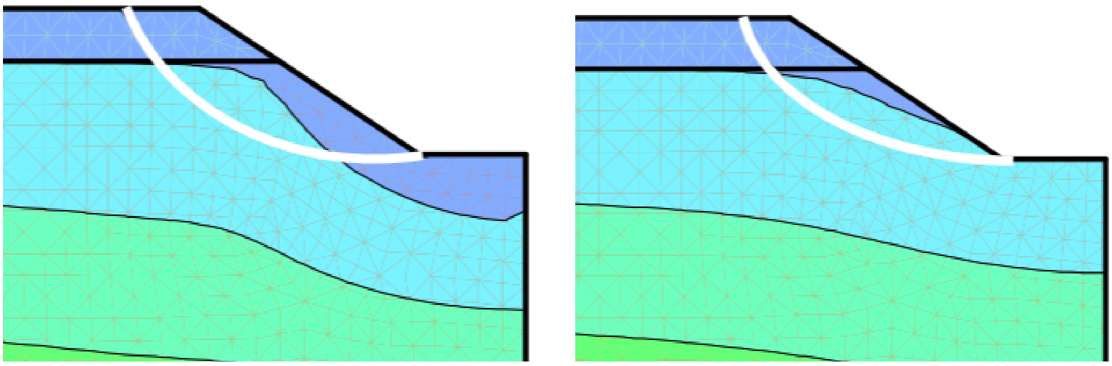

(a) Critical slip surface identified at 1 day after excavation.

(b) Critical slip surface identified at 300 days after excavation.

Figure 4.11: Critical slip surfaces corresponding to the shear resistance distributions shown in Figure 4.12.

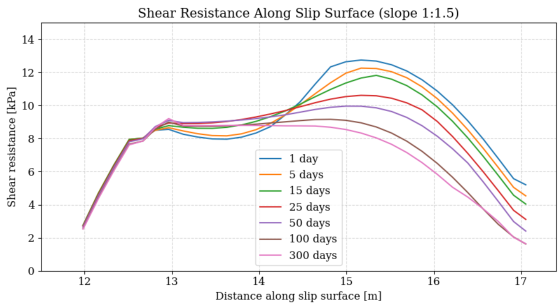

(a) The shear resistance along the slip surface corresponds to the critical slip surface identified 1 day after excavation.

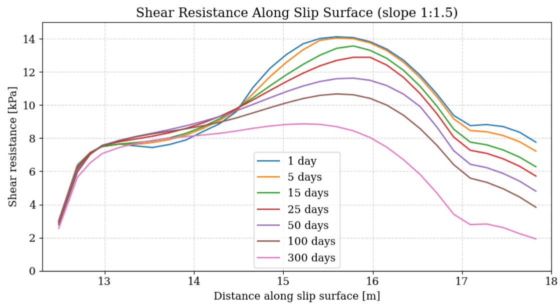

(b) The shear resistance along the slip surface corresponds to the critical slip surface identified 300 days after excavation.

Figure 4.12: Shear resistance along the same slip surface for different times after excavation for slope 1:1,5.

The behaviour differs more significantly for the 1:2 slope shown in Figures 4.13 and 4.14. In this case, the critical slip surface identified at 1 day after excavation is considerably deeper than the critical slip surface identified at 500 days, which becomes much shallower and concentrated closer to the slope surface. The shear resistance distribution along the deep slip surface at early times remains relatively high and uniform over a large portion of the slip surface, indicating that much of the slip surface behaves under predominantly undrained conditions shortly after excavation. As time progresses and pore pressures dissipate, the critical mechanism transitions towards a shallower slip surface where the shear resistance decreases more substantially near the slope toe. This suggests that the stability behaviour for the flatter slope is more strongly influenced by the transition from undrained to drained conditions over time.

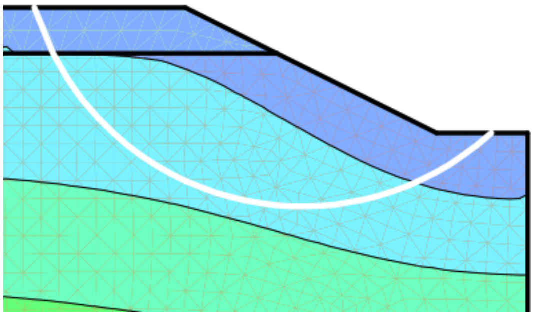

(a) Critical slip surface identified at 1 day after excavation.

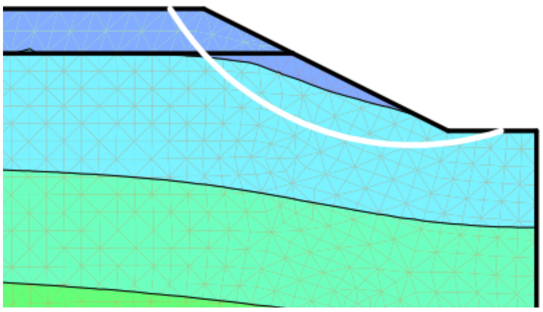

(b) Critical slip surface identified at 500 days after excavation.

Figure 4.13: Critical slip surfaces corresponding to the shear resistance distributions shown in Figure 4.14.

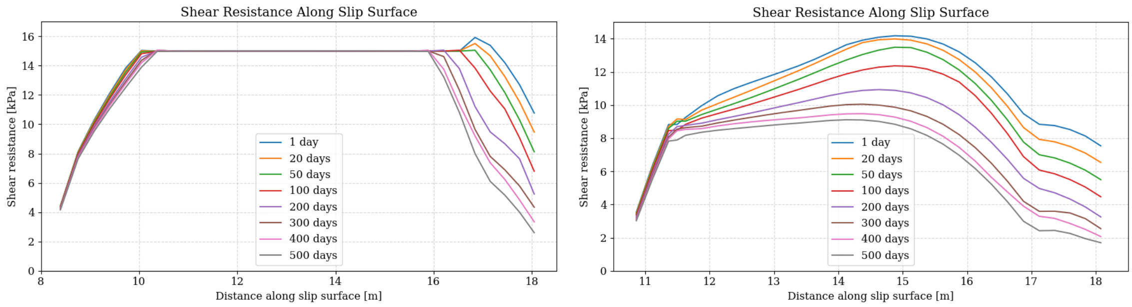

(a) The shear resistance along the slip surface corresponds to the critical slip surface identified 1 day after excavation.

(b) The shear resistance along the slip surface corresponds to the critical slip surface identified 500 days after excavation.

Figure 4.14: Shear resistance along the same slip surface for different times after excavation for slope 1:2.

4.4 Factor of safety evolution during the undrained to drained transition

Figure 4.15 presents the FoS as a function of time after excavation for three analysed cases: slope inclination of 1:1, 1:1,5 and 1:2 with the same excavation depths of 2,75 m. The consolidation coefficient is defined as $c_v = kE/\gamma_w$ [$\mathrm{m^2\,s^{-1}}$]. Results are presented in three complementary plots: (a) FoS agains time in days, (b) FoS against the dimensionless time factor $T_v = c_v t/H_e^2$, where $H_e = H$ is the excavation depth adopted as the drainage path length assuming one way drainage, and (c) normalised FoS against time factor.

Figure 4.15a) shows that all three cases exhibit a continuously decreasing FoS with time after excavation, reflecting the transition from undrained conditions immediately after excavation towards fully drained conditions as the negative excess pore pressure dissipate. Of the three cases, the slope 1:2 (red) maintain the highest FoS throughout, with an initial value of 1,75 decreasing to 1,31 at a fully drained value after approximately 3000 days. The case with slope inclination of 1:1,5 (orange) starts at an initial value of 1,45 and decreases to 1,12. Slope 1:1 (blue) begins at a lower short-term value of 1,26, as expected given the steeper slope angle, and reaches a long-term value at 1,05. Notably, the flatter slopes requires significantly more time to converge to drained conditions compared to the steeper slopes, where the steepest have reached almost drained conditions at $t = 200$ days and the flattest at $t > 500$ days.

Figure 4.15b) presents the results in terms of the time factor T_v enabling a geometry independent comparison of the consolidation process. All cases exhibit a characteristic behaviour, an initial plateau at low T_v corresponding to the undrained short-term conditions, followed by a decrease in FoS and a final plateau at high T_v representing the drained long-term conditions. The slope 1:2 maintain the highest FoS throughout as explained above with a markedly delayed transition. The initial undrained plateau is maintained up to approximately $T_v \approx 10^{-1}$, after which the FoS decreases, with the transition completing between $T_v = 10^0$ and $T_v = 10^1$. In days this relates to 20-400 days. The 1:1,5 slope has its transition occurring in the range of $T_v \approx 10^{-1}$ to 10^1 which in time corresponds to around 20 to 180 days. The transition for the 1:1 slope occurs earlier, in the range $T_v \approx 10^{-2}$ to 10^0, which in time corresponds to 5 to 150 days. Figure 4.15c) shows the normalized FoS, defined as:

$$\text{Normalized FoS} = \frac{FoS(t) - FoS_{\text{1d}}}{FoS_{t_{\text{drained}}} - FoS_{\text{1d}}} \tag{4.1}$$

where $t = 1$ day represents the undrained short-term condition (normalized value=0) and t_{drained} the final fully drained value for each respective case (normalized value=1). This normalization highlights the relative rate of transition from undrained to drained conditions, independent of the absolute FoS values. Undrained conditions are assumed to prevail until the plateau in the factor of safety curve ends, corresponding to approximately a 5% reduction from the initial undrained value. Based on this assumption, the results in Figure 4.15c) indicate that the short-term undrained condition persists for approximately 15 days for both the 1:2 slope and the 1:1,5 slope before transitioning to partially drained conditions. The corresponding period for the 1:1 slope is approximately 5 days.

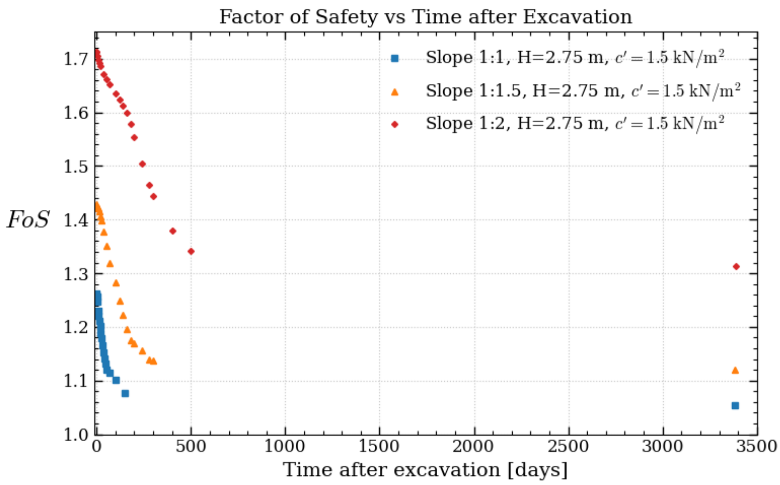

(a) Factor of safety vs time after excavation.

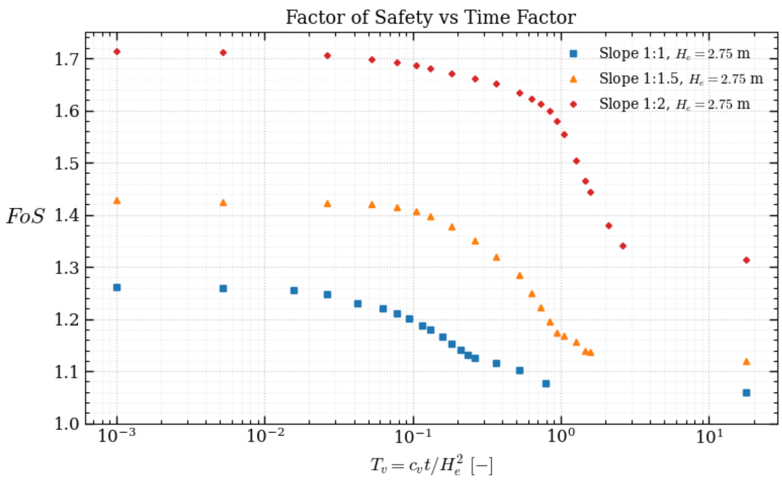

(b) Factor of safety vs time factor.

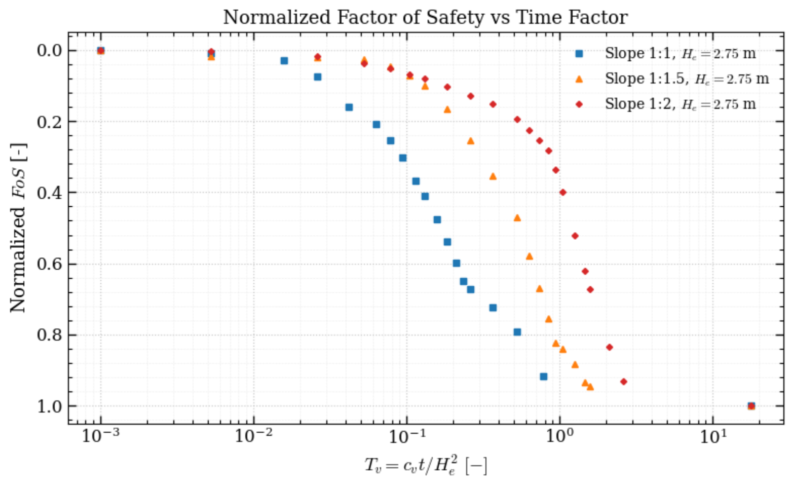

(c) Normalized factor of safety vs time factor.

Figure 4.15: Gradual transition from undrained to drained conditions with combined in SLOPE/W.

Table 4.1 summarises the characteristic transition times for the three analysed slopes. For the steepest slope (1:1), the undrained assumption remains valid for approximately 5 days after excavation after which the pore pressure begin to dissipate at a rate sufficient to the influence stability. The 50 % and 95 % FoS reduction are reached at 30 and 150 days respectively. For the 1:1,5 slope and the flattest slope 1:2, the undrained assumption holds for approximately 15 days in both cases, reflecting a similar initial consolidation rate despite the difference in geometry. However, the subsequent transition progresses more slowly for the flatter slope, with 50 % of the FoS reduction occuring at 100 days for the 1:1,5 slope compared to 200 days for the 1:2 slope, and almost drained conditions (95%) reached at 300 and 500 days respectively.

Table 4.1: Characteristic times for the transition from undrained to drained conditions after excavation.

Geometry	**Undrained assumption [days]**	**50% FoS reduction [days]**	**95% FoS reduction [days]**
Slope 1:1	5	30	150
Slope 1:1,5	15	100	300
Slope 1:2	15	200	500

4.4.1 Comparison of factor of safety for different methods

Table 4.2 presents the factor of safety obtained for different slope geometries and analysis conditions using two different analysis approaches. Method 1 consists of analyses performed in SLOPE/W using the Mohr–Coulomb model for the undrained and drained analyses, and the Combined *S=f(depth)* approach for the combined analysis. In Method 1, pore pressures are represented using manually drawn piezometric lines and no suction contribution is included. Method 2 consists of analyses performed using imported pore pressures from PLAXIS 2D together with the Shear-Normal Function approach in SLOPE/W for the undrained, combined, and drained analyses. The undrained analysis is only done for Method 1 because the effect from negative pore pressure will not have any impact on the FoS for the Shear-Normal Function. The first time step for Method 2 represents the first day after excavation, while the *final day* represent the stage at which the factor of safety curve begins to converge towards fully drained conditions.

For the undrained analysis, both methods yield the same results. For the combined analysis, a notable discrepancy is observed, where Method 1 yields considerably lower FoS values while Method 2 produces higher FoS values. Furthermore, the combined analysis results obtained using Method 1 are identical to the drained analysis results. This is because Method 1 does not account for time-dependent pore pressure dissipation or the contribution of negative pore pressures. Consequently, the analysis assumes fully drained conditions throughout the entire period, resulting in a factor of safety equal to the drained value. The FoS obtained using Method 2 at the final day of the combined analysis approaches the values obtained from the drained analysis.

Table 4.2: FoS for different slope geometries and analysis conditions using Method 1 (Mohr–Coulomb and Combined *S=f(depth)* approach with drawn piezometric lines) and Method 2 (SNF with imported pore pressures from PLAXIS)

Analysis type	**Method**	**1:1**	**1:1,5**	**1:2**
Undrained	1	1,623	1,744	1,799
Combined	1	0,687	0,803	1,005
	2 (day 1)	1,262	1,425	1,713
	2 (final day)	1,077	1,131	1,323
Drained	1	0,687	0,803	1,005
	2	1,055	1,120	1,313

4.5 Sensitivity analysis

This section presents the results of the sensitivity analysis conducted for the five parameters: effective cohesion, undrained shear strength, Young's modulus, permeability, and effective friction angle. In each analysis, only the parameter under investigation is varied while all other input parameters are kept at their reference values, as defined in Table 3.5. It should be noted that for the effective cohesion and the Young's modulus, the fill material parameters are also adjusted accordingly, as described in Table 3.5.

4.5.1 Effective cohesion, c'

Figure 4.16 shows the variation of the FoS with time after excavation for three values, $c' = 1,2kN/m^2$, $c' = 1,5kN/m^2$ and $c' = 2,0kN/m^2$, for a slope inclination of 1:1 and an excavation depth of 2,75 m. It is evident that all three cases follow a similar trend, with an initially elevated FoS that decreases continuously until an approximate long term equilibrium is reached at around 75-100 days after excavation. At t=0 FoS is approximately 1,16, 1,27 and 1,32 for $c' = 1,2, 1,5$, and $c' = 2,0kN/m^2$, respectively, indicating a clear positive relationship between cohesion and initial stability. The most pronounced reduction in FoS occurs within the first 50 days, after which the rate of decrease diminished and the curves begin to level off. At a long-term equilibrium state around 100 days, all three curves started to converge towards a range of 1,10-1,12, indicating that the influence of cohesion on stability becomes considerably less significant over time. It can be seen that the sensitivity of FoS to changes in c' is greatest immediately after excavation, where a difference of $0,8kN/m^2$ in cohesion corresponds to a difference of approximately 0,16 in FoS. This difference reduces to less than 0.02 at long-term equilibrium.

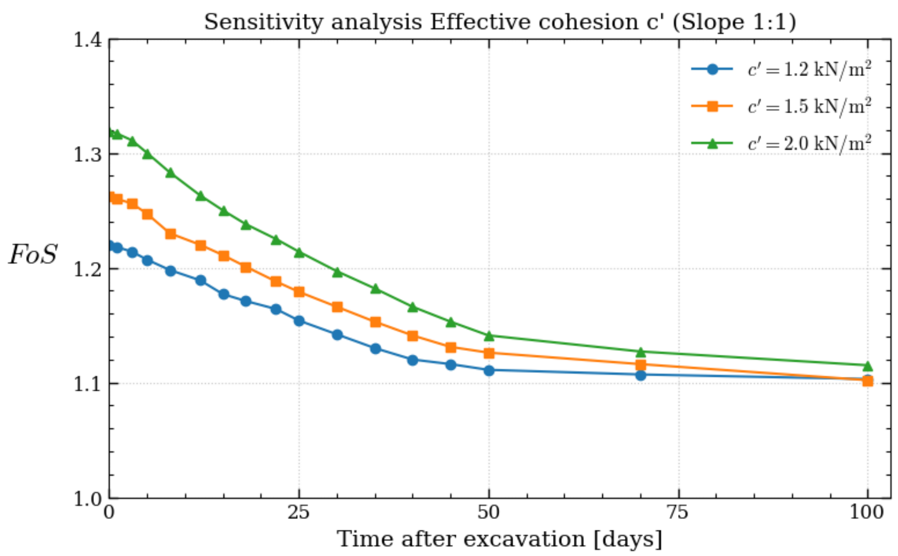

Figure 4.16: Factor of safety vs time after excavation for a sensitivity analysis of the effective cohesion. The fill cohesion is adjusted accordingly. All other parameters are kept at their reference values.

4.5.2 Undrained shear strength, c_u

Figure 4.17 shows the variation of FoS with time after excavation for three values of undrained shear strength, $c_u = 12$, 15 and 20 kPa, for a slope inclination of 1:1 and an excavation depth of 2,75 m. All three cases show a decreasing trend with time, where the FoS gradually reduces as the analysis approaches the long-term condition.

At the initial stage, the lowest value of c_u gives a clearly lower FoS, with an initial value of approximately 1,17 for $c_u = 12$ kPa compared with approximately 1,26 for both $c_u = 15$ kPa and $c_u = 20$ kPa. The difference between $c_u = 15$ kPa and $c_u = 20$ kPa is negligible throughout the analysis, indicating that an increase in undrained shear strength above 15 kPa does not further affect the calculated stability in this case. This is because the Shear-Normal Function is limited to a maximum undrained shear strength of 15 kPa. Meaning that increasing c_u beyond 15 kPa does not affect the calculated FoS. The largest difference between the curves is observed shortly after excavation. With time, the curves gradually converge, and at around 100 days all cases approach a similar FoS of approximately 1,10. This indicates that the influence of c_u is most pronounced during the early stages after excavation, while its effect becomes less significant as the response approaches the long-term drained condition.

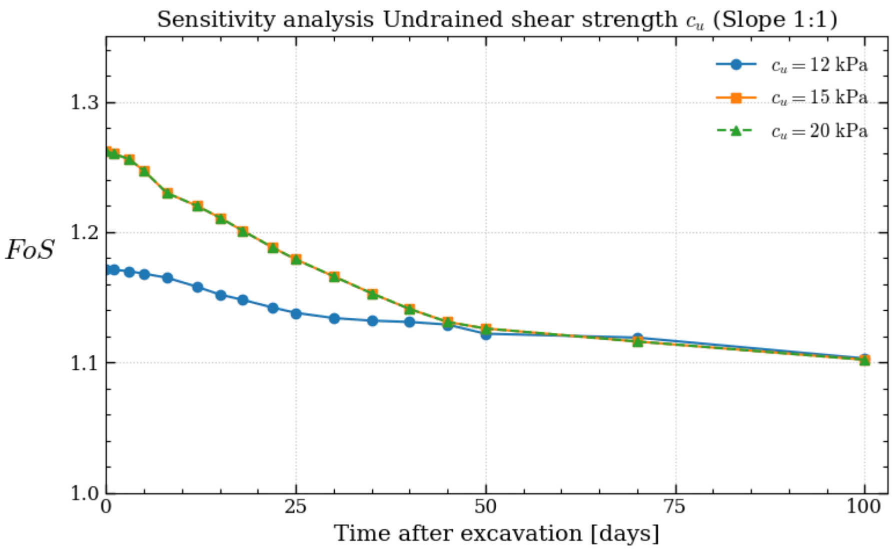

Figure 4.17: Factor of safety vs time after excavation for a sensitivity analysis of the undrained shear strength. All other parameters are kept at their reference values.

4.5.3 Young's modulus, E

In Figure 4.18, the variation of FoS with time after excavation is presented for three different values of E-modulus for a slope inclination of 1:1. The tested values are $E = 4500, 7500$ and $15000 kN/m^2$. In contrast to the sensitivity analysis of c' and c_u, the initial values of FoS at $t = 0$ are nearly identical across all three cases, at approximately 1,26, indicating that the stiffness parameter has a negligible influence on stability immediately after excavation. The primary effect of E is instead evident in the rate at which FoS decreases over time. This behaviour is physically expected, as the stiffness influences the coefficient of consolidation, c_v, which governs the rate of pore pressure dissipation. According to $c_v = kE/\gamma_w$, an increase in stiffness results in a higher consolidation coefficient and consequently a faster transition from undrained to drained conditions. For the highest stiffness, $E = 15000 kN/m^2$, FoS drops rapidly and reaches long term equilibrium at approximately $t = 40$ days. For the intermediate value $E = 7500 kN/m^2$, convergence is reached at approximately $t = 70$ days. For the lowest stiffness $E = 4500 kN/m^2$ the decrease is more gradual and drainage takes longer time. At $t = 100$ days converge is not even reached yet. It can be seen that all three curves converge towards essentially the same long-term FoS of approximately 1,1, regardless of the assumed stiffness. This indicates that E does not significantly affect the long-term stability of the slope, but rather governs the rate of pore pressure dissipation and thus the speed at which the long-term consolidation is reached.

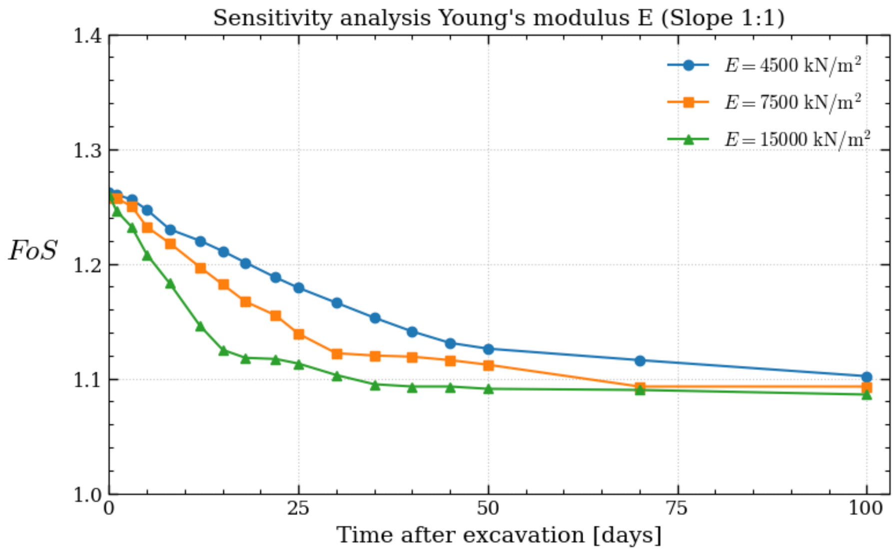

Figure 4.18: Factor of safety vs time after excavation for a sensitivity analysis of the E-modulus. The fill E-modulus is adjusted accordingly. All other parameters are kept at their reference values.

4.5.4 Permeability, k

Figure 4.19 shows the variation of FoS with time after excavation for three values of permeability, $k = 1 \times 10^{-9}$, 1×10^{-8}, and $1 \times 10^{-7} m/s$ for a slope inclination of 1:1 and the depth of 2,75 m. The results show a pattern consistent with those observed for the E-modulus, which is physically expected given that both parameters govern the consolidation coefficient $c_v = kE/\gamma_w$. As with the variation of E, the initial FoS at $t = 0$ differs only marginally between the three cases, at approximately 1,25, while the primary effect of k is on the rate of FoS reduction over time. For the highest permeability of $k = 1 \times 10^{-7} m/s$, the FoS decreases rapidly and reaches long-term equilibrium at $t = 15 - 20$ days, stabilizing at a value of 1,1. For $k = 1 \times 10^{-8} m/s$, equilibrium is reached at approximately $t = 20 - 30$ days at a similar long term value. For the lowest permeability $k = 1 \times 10^{-9} m/s$, the decrease is considerably more gradual and a full long-term equilibrium has not really been reached within the 70 days period, with FoS still at approximately 1,12 at $t = 70$ days.

It is evident that all three cases converge towards the same long-term FoS, confirming that permeability does not influence the drained stability of the slope. Rather k controls the rate of pore pressure dissipation following excavation and the speed at which the long-term condition is approached. The results further confirm the findings from the sensitivity analysis of E and together they highlight that the consolidation characteristics of the soil are a key factor in determining how quickly a slope transitions from its short-term to its long-term stability state.

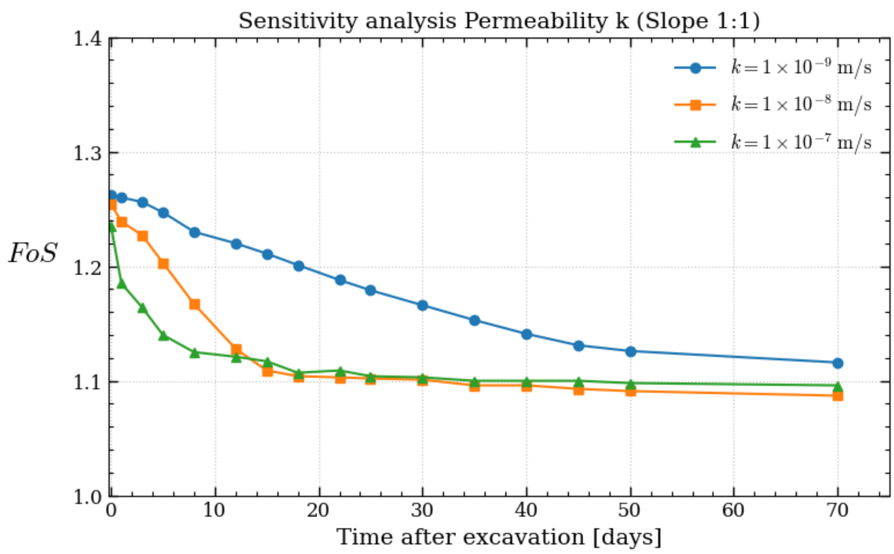

Figure 4.19: Factor of safety vs time after excavation for a sensitivity analysis of the permeability. All other parameters are kept at their reference values.

4.5.5 Effective friction angle, ϕ'

Figure 4.20 presents the variation of FoS with time after excavation for three different values of effective friction angle, $\phi' = 27°$, $30°$, and $33°$, for a slope inclination of 1:1 and excavation depth of 2,75 m. Unlike E and k, the friction angle has a pronounced influence on FoS throughout the entire consolidation period, with the three curves maintaining a persistent separation from $t = 0$ to $t = 100$ days. At $t = 0$, the FoS is approximately 1,16, 1,27 and 1,38 for $\phi' = 27°$, $30°$, and $33°$ respectively. It can be seen that ϕ' exerts a significant influence on both the short-term and long-term stability of the slope, with the gap between the curves remaining largely constant over time. At $t = 100$ days, the FoS has decreased to approximately 1,05, 1,10 and 1,16 $\phi' = 27°$, $30°$, and $33°$, respectively, and none of the curves appear to have reached fully long-term equilibrium within the studied 100 days.

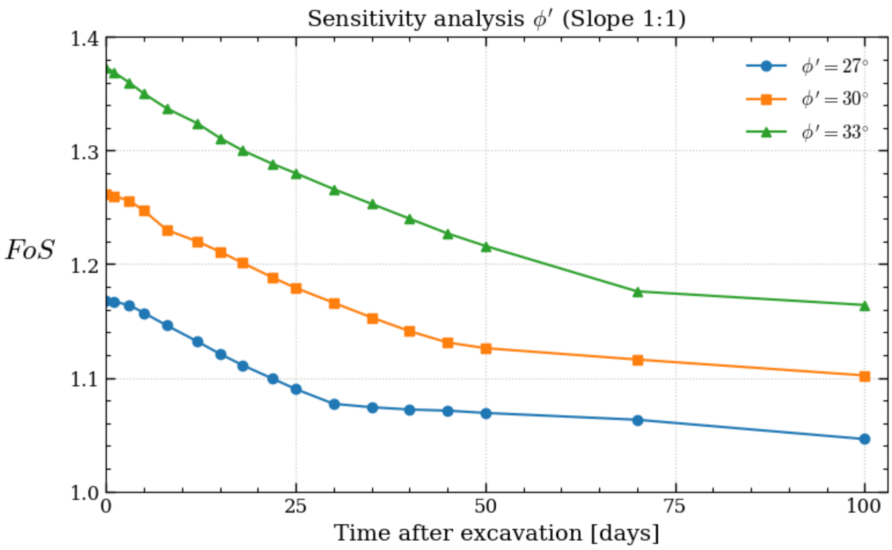

Figure 4.20: Factor of safety vs time after excavation for a sensitivity analysis of the effective friction angle. All other parameters are kept at their reference values.

5
Discussion

This chapter discusses the methodology and the main findings obtained from the numerical analyses. The results are interpreted in relation to the theoretical framework presented in Chapter 2, with particular focus on the development and dissipation of negative pore pressures, the transition from undrained to drained conditions, and the influence of slope geometry on stability over time. The limitations and uncertainties associated with the modelling approach, parameter selection and assumptions adopted in the analyses are also addressed. Finally, the results are compared with Swedish recommendations for temporary excavations in clay, in order to evaluate how the numerical analyses relate to current geotechnical practice.

5.1 Modelling approach and limitations

The analyses were carried out using a combined numerical approach, where finite element modelling in PLAXIS 2D was used to simulate the time-dependent pore pressure response following excavation, and limit equilibrium analyses in SLOPE/W were used to evaluate the corresponding factor of safety. While this approach enabled detailed investigation of the transition from undrained to drained conditions, several modelling choices and simplifications warrant discussion.

All material in this study was modelled using the Mohr-Coulomb constitutive model. This model is a linear elastic perfectly plastic formulation that requires relatively few input parameters and is simple to implement. Although widely used and numerically efficient, the model has limitations when applied to soft clay. For example it does not capture the non-linear stress-strain response or the variation in stiffness with stress level. More advanced models would describe the soil behaviour more realistically. However, given that the primary objective of using FEM in this study was to evaluate the pore pressure distribution with time rather than predict exact deformations, the Mohr-Coulomb model is considered as an appropriate approximation for this type of analysis. A key aspect of the methodology was the transfer of nodal pore pressure distribution from PLAXIS 2D to SLOPE/W for each analysed time step, using linear interpolation via the spatial function method. The overall pore pressure patterns reproduced well between the two programs, as illustrated in Figure 4.1. However, linear interpolation may introduce local inaccuracies in regions where pore pressure gradients are steep, particularly near the slope surface and excavation bottom. Krigged interpolation could potentially provide a smoother representation in these zones, but given the amount and density of the exported nodal data, linear interpolation was considered sufficiently accurate.

Another methodological aspect that should be considered is the characteristic drainage length used in the calculation of the time factor T_v. In this study, the excavation depth H_e was adopted as the drainage length, assuming that the excavation depth governs the characteristic consolidation process controlling the dissipation of negative pore pressures. This simplification was considered appropriate for comparing the different slope geometries analysed in this study. However, the effective drainage length in reality may vary depending on the geometry of the critical slip surface, the location of the negative pore pressure zones, and the assumed drainage boundaries. Alternative definitions of H_e could therefore produce somewhat different rates of consolidation and transition times between undrained and drained conditions. The selected approach should therefore be regarded as an approximation intended to provide a consistent basis for comparison between the analysed cases.

The material parameters were selected to be representative of soft clays commonly encountered in Sweden, consistent with values reported in the literature and Swedish geotechnical guidelines. The undrained shear strength of 15 kPa corresponds to an average value specified in the recommended excavation geometries by Lundström et al. (2015), the effective friction angle of 30° falls within the commonly reported range for Scandinavian clays, and the effective cohesion of 1,5 kPa corresponds to the empirical approximation $c' = 0.1cu$ used in Swedish practice. While these values are considered representative and consistent with empirical data, the sensitivity analysis highlights the importance of obtaining reliable input parameters through site investigations and laboratory testing. It could be seen in the sensitivity analysis that the friction angle was found to exert the most significant influence on the factors of safety throughout the consolidation period, highlighting the importance of determining the parameter accurately.

5.2 Generation and dissipation of negative pore pressures

The pore pressure development obtained from PLAXIS 2D showed a clear pattern with negative pore pressures concentrated along the slope surface and at the excavation bottom immediately following excavation, which is consistent with the theoretical framework in Chapter 2. The comparison between pore pressure distribution in PLAXIS 2D and SLOPE/W shown in Figure 4.1 indicates that the imported pore pressure conditions in SLOPE/W reasonably reproduce the results from the Finite Element modelling approach used in this study.

The gradual dissipation of the negative pore pressures observed in the analyses, see Figure 4.2, 4.3 and 4.4 is consistent with the theoretical framework presented in Sections 2.4.3 and 2.5.2. As described in Section 2.4.3, excavation causes an immediate undrained response that generates temporary negative excess pore pressures. With time, these pore pressures dissipate through consolidation, as described in

Section 2.5.2, causing the pore pressure distribution to gradually approach drained conditions.

For all analysed geometries, clear zones of negative pore pressure were visible near the slope surface and excavation bottom immediately after excavation. As time progressed, these zones gradually decreased in both magnitude and extent, while the pore pressure contours became smoother and more uniform. This development indicates that the temporary suction generated by excavation continuously decreases with time as water flows towards the excavation and the pore pressure distribution approaches hydrostatic conditions, consistent with the consolidation process described in Section 2.4.3.

A notable difference in pore pressure development was observed between the different geometries. This can be attributed to the greater volume of soil being unloaded during excavation. For flatter slopes, a larger volume of soil is removed which leads to greater stress relief and consequently larger negative pore pressures developing over a wider area of the slope. As a result, it takes longer for these pressures to dissipate and for the soil to reach equilibrium. For the steep 1:1 slope, the negative pore pressure dissipated relatively quickly and the pore pressure contours had largely converged already at approximately 100 days. In contrast, the 1:1,5 slope showed a slower dissipation process, where negative pore pressures were still visible near the slope surface at 300 days. The 1:2 slope showed the slowest overall development, with the pore pressure distribution continuing to evolve up to approximately 500 days before approaching convergence. The selected “final day” for each geometry therefore corresponds to the stage where the majority of the negative pore pressures had dissipated and the analysed response curves had largely converged, indicating that the pore pressure distribution was approaching fully drained conditions.

An observation that was made was the local pore pressure shape visible near the crest of the 1:1,5 slope at 1 day after excavation, see Figure 4.3, where the negative pore pressure contours extended further into the slope compared to the other geometries. A similar, but not that clear pattern was also observed for the 1:2 slope (4.4). The reason for this behaviour is not entirely clear, but it may be related to the stress redistribution immediately following excavation, where both vertical unloading beneath the excavation and horizontal stress relief near the slope influence the pore pressure response, as discussed in Section 2.4.3. As noted earlier, these slope geometries involve greater stress relief, meaning greater stress changes that can take longer to redistribute. The result suggests that the geometry of the slope influences not only the rate of pore pressure dissipation, but also the initial distribution of the negative pore pressures immediately after excavation.

5.3 Influence of negative pore pressures, ϕ^b, on short-term stability

The results clearly show that the negative pore pressures and the angle ϕ^b has a significant influence on short-term stability after excavation, but no influence on long-term drained stability. For all geometries, the curves converge towards a common FoS value once the negative pore pressures had dissipated which is confirming that the contribution of suction to shear strength is temporary in such cases as in this study. In practice, this implies that an excavation that is open for a short time may benefit from the additional stability provided by suction, but this margin should not be relied upon longer than some days, as shown in the results, since it decreases continuously with time. Furthermore, the combined analysis using the material model $S = f(depth)$ in SLOPE/W overlapped the curve $\phi^b = 0°$ throughout the consolidation period. This indicates that this model does not account for any contributions from negative pore pressures to shear strength, which is an important limitation and may lead to an underestimation of the short-term stability. By importing pore pressures from PLAXIS 2D to SLOPE/W and allowing the contribution from ϕ^b, a more representative description of the short-term behavior and the stabilizing effect of temporary slopes could be achieved.

In this study ϕ^b was set to 15 degrees, corresponding to half of the effective friction angle ϕ', following the recommendation by Seequent (2022). This value is an assumption, as ϕ^b varies between soils depending on factors like soil type, degree of saturation, suction level and stress conditions, as described in chapter 2.4.2. It should however be noted that while ϕ^b was kept constant throughout the analyses, the contribution of suction to shear strength was not constant but varied over time, since the magnitude of the negative pore pressures changed with each time step as consolidation progressed. In this sense, the time-dependent response of suction contribution to the factor of safety is captured through the change in pore pressure distribution imported from PLAXIS 2D. The effect of varying ϕ^b is further illustrated in Section 4.2, where higher values of ϕ^b results in higher short-term FoS. To avoid overestimating the contribution of negative pore pressures to shear strength, a lower recommended ϕ^b was adopted in this study. This ensures that the stabilising effect of temporary suction is included in the assessment without being overstated.

5.4 Shear resistance along critical slip surface

The results presented in Section 4.4 show how the distribution of shear resistance along the critical slip surface evolves with time, and where the reduction in stability is most pronounced during the transition. For the steeper slopes 1:1 and 1:1,5, the critical slip surface geometry remained relatively stable between the early and late time steps, indicating that the location and shape of the governing failure mechanism does not change that much with time. The shear resistance decreased progressively along most of the slip surface, with the most pronounced reduction occurring near the passive zone close to the slope toe. This is consistent with the theory described in Section 2.4.3, where suction generated by excavation unloading is most concentrated near the slope surface and excavation bottom. As this suction dissipates, the effective stresses in the passive zone decrease towards their drained values which is reducing the available shear resistance in this region. The active zone near the crest was comparatively less affected by time-dependent changes.

The behaviour for the 1:2 slope differs more significantly. Here the critical slip surface moved from a deep to a shallower position between short-and long-term, reflecting a transition from an undrained to a drained-governed failure mechanism over time. Since the slip surface for the flatter slope is initially deeper and more influenced by undrained conditions compared to the steeper geometries, this has a notable effect on the distribution of shear resistance, as illustrated in Figure 4.14a. With the effective cohesion set to c'=1,5 kPa, consistent with the empirical relationship $c' = 0.1c_u$ (Larsson et al., 2007; Skredkommissionen, 1995; Trafikverket, 2011), the shear-normal function defined in SLOPE/W imposes an upper limit on the available shear strength equal to the undrained shear strength of c_u=15 kPa. For the flatter slope under early undrained conditions, the drained Mohr-Coulomb formulation would predict shear strength exceeding this limit along parts of the deeper slip surface. Since the combined shear strength envelope caps the mobilised resistance above 15 kPa when distributed along the slip surface, it also limits some of the stability, which also explains the shape of the curves observed in Figure 4.14a. This discrepancy arises from how the two programs handle shear strength in a different way. As described in Section 2.10.2, drainage type Undrained A does not impose an upper limit on the mobilised undrained shear strength, which means that the shear strength along parts of the slip surface can exceed c_u in PLAXIS 2D. However, when the pore pressures are imported into SLOPE/W, the combined shear-normal function controls this by capping the available shear strength at c_u= 15 kPa. The clay is therefore still constrained to its defined undrained shear strength in the stability assessment in SLOPE/W and this difference should be viewed as a consequence of the two programs.

5.5 The undrained to drained transition and its implications for stability assessment

The results presented in Section 4.3 demonstrate that the factor of safety decreases with time after excavation as the negative pore pressures dissipate and the pore pressure distribution gradually approaches drained conditions. This behaviour is consistent with the theory presented in Sections 2.4.3 and 2.5.2, where excavation unloading initially generates negative excess pore pressures under undrained conditions. These negative pore pressures temporarily increase the effective stress and thereby contribute to an increased shear strength directly after excavation. As consolidation progresses, the negative pore pressures dissipate, which is reducing the stabilising effect and resulting in a lower factor of safety.

A clear difference was observed between the traditional method of calculating combined analysis and the method in this study, including imported pore pressures from PLAXIS 2D. The traditional method resulted in significantly lower factors of safety, compared to this study's method with pore pressures (Table 4.2). Furthermore, the traditional method produced results that closely resembled the drained conditions already from the beginning of the analysis. This indicates that the traditional combined analysis does not capture any stabilising contribution from suction compared to the method of importing pore pressures to SLOPE/W. As described in Section 2.8, the combined analysis selects the minimum of the fully drained and undrained shear strength, which means that the temporary increase in shear strength caused by suction is not reflected in the calculated stability. As a consequence, the short-term stability may be underestimated if combined stability analysis is required as calculation approach. On the other hand, for the method used in this study with imported pore pressures, it showed a clear time-dependent reduction in factor of safety. Immediately after excavation, the factor of safety was significantly higher due to the contribution from negative pore pressures together with the suction friction angle ϕ^b. As pore pressure dissipate with time, the factor of safety gradually converged towards the long-term drained value as could be seen in Table 4.2. This confirms that the stabilising effect of suction is temporary and highly dependent on the transient pore pressure conditions within the slope.

A clear relationship between slope inclination and both the magnitude and rate of stability transition is evident from the results. Steeper slopes exhibit lower initial factor of safety and converge more rapidly towards drained conditions, while flatter slopes maintain higher short-term values and require considerably longer times to reach the drained state, see Table 4.1. This is an consequence of the increased driving force in relation to the stabilising force acting on the sliding mass as inclination increases: a steeper slope causes a larger portion of the soil weight to act on the driving side of the failure surface relative to the centre of rotation, thereby increasing the mobilised shear stress in relation to the available frictional resistance. This results in a lower factor of safety for steeper geometries, independent of the drainage conditions. Beyond the mechanical effect of slope inclination on force equilibrium, slope geometry also strongly influences the rate at which pore pressure dissipate and stability evolves over time. Steeper slopes transition more rapidly towards drained conditions and this behaviour can partly be explained by following factors. The critical slip surface is shallower and more concentrated within the zone of negative excess pore pressure near the slope and excavation bottom, meaning that suction constitutes a large proportion of the shear resistance mobilised along the slip surface. When this suction dissipates, the slope consequently loses a significant share of its available shear strength over a short period, leading to rapid reduction in factor of safety. Also the shorter drainage path in steeper geometries allow pore pressures to equilibrate more quickly. For flatter slopes, the slip surface extends over a greater horizontal distance and reaches further into the clay mass, where the influence of the suction zone is less pronounced. A larger proportion of shear resistance is therefore governed by drained effective stresses, reducing the relative influence of suction on overall stability. Combined with the larger volume of soil subject to unloading, this delays the dissipation process and prolongs the transition towards drained conditions.

Taken together, quantifying how long a clay slope can be assumed fully undrained remains challenging, and Figure 4.15c provides useful insight into this for the three geometries with H=2,75m. For the 1:1 slope, the normalised FoS begins to deviate from zero after approximately 5 days, beyond which a combined analysis should be applied. For the 1:1,5 and 1:2 slopes, the undrained plateau persist for approximately 15 days before the transition begins. However, this similar onset of transition for the 1:1,5 and 1:2 slopes does not mean they behave equivalently beyond this point. For the 1:1,5 slope, the curve drops relatively steeply once it departs from the undrained state, whereas for the flatter 1:2 slope the curve remains comparatively flat until approximately 50 days, after which the steepest decline occurs. This difference reflects the proportion of shear resistance governed by suction vs drained effective stresses along each slip surface. For slope 1:1,5, suction constitutes a larger share of the total shear resistance, and its dissipation therefore produces a rapid reduction in factor of safety. For the flatter 1:2 slope, the slip surface extends further into the clay where drained shear strength already contributes from the outset, partially compensating for the loss of suction and allowing the slope to maintain relatively higher stability for a longer period. An additional factor that may contribute to the similar undrained plateau duration observed for the 1:1,5 and 1:2 slopes is related to the upper limit imposed on the mobilised shear resistance by the combined material model in SLOPE/W, to represent a clay with c_u=15 kPa. For the flatter 1:2 slope, where the deeper undrained slip surface results in higher mobilised shear strengths, the upper limit imposed by the Shear-Normal Function constrains part of the available stability, see Figure D.1. Increasing the upper limit of the Shear-Normal Function results in a shallower critical slip surface during the first days after excavation, together with higher values of FoS, see Figure D.2 and D.3. Nevertheless, the results remains representative of a clay with c_u=15 kPa, which was the intended soil condition for comparison.

5.6 Influence of material parameters on stability

The sensitivity analysis provides insight into which parameters have the greatest influence on stability and how parameter uncertainty affects the results, both in short-term and long-term.

The effective cohesion c' had the greatest influence on stability immediately after excavation. This influence diminished with time as the negative pore pressures dissipated and effective stresses decreased towards their long-term drained values. This suggests that the stabilising effect provided by cohesion becomes less dominant with time compared to the frictional component governed by effective stresses. This behaviour does not reflect a reduction in c' itself, but rather that the tested range of c' values is small in absolute terms. As the conditions transition towards drained conditions, the ϕ' dominates over the cohesive contribution. Since ϕ' is the same for all three curves, the long-term drained stability converges towards the same value.

The sensitivity analysis of the undrained shear strength c_u revealed that increasing the cap from 15 kPa to 20 kPa in the shear-normal function in SLOPE/W had no effect on the calculated factor of safety, as the two cases produced identical results throughout the entire analysis, see Figure 4.16. This can be attributed to the fact that the pore pressures were imported from PLAXIS 2D, where the clay was modelled using drained strength parameters calibrated to represent a material with an undrained shear strength of approximately 15 kPa. Consequently, the mobilised shear strength in SLOPE/W never exceeded this value regardless of the imposed cap, rendering the increase to 20 kPa superfluous. When the cap was instead reduced to 12 kPa, the limit became active and constrained the mobilised shear strength below what the clay would otherwise develop, resulting in a lower factor of safety.

The Young's modulus E (Figure 4.18) and permeability k (Figure 4.19) showed a similar effect on the results, which is expected following the since both parameters govern the consolidation coefficient c_v, described in chapter 2.5.2. Neither parameter had any notable influence on the initial FoS at $t = 0$, nor on the final long-time value. Their primary effect was on the rate at which the FoS decreased over time, with higher values of E and k leading to faster pore pressure dissipation and therefore a more rapid transition towards drained conditions. This also highlights that E and k have a significant influence on how long the clay slope can be considered undrained before transitioning to drained, which makes it important to be aware of the sensitivity to these parameters. In particular, for clays with high stiffness or high permeability, undrained analyses are only valid for very short periods following excavations. In such cases, relying solely on an undrained analysis without considering the time-dependent development for the factor of safety could lead to non-conservative assessment of the permissible duration of the excavation, as the actual factor of safety may decrease more rapidly than assumed.

The effective friction angle ϕ' showed the most significant and persistent influence on the factor of safety throughout the consolidation period (Figure 4.20). Unlike the other parameters, the separation between the curves remained nearly constant over time, indicating that ϕ' governs both short-term and long-term stability. This highlights ϕ' as one of the most critical parameters in stability assessment. It should however be noted that the rate at which the factor of safety decreases over time is the same regardless of the assumed value of ϕ', as the curves maintain a constant separation throughout the consolidation period. This implies that ϕ' does not significantly influence how long the slope can be considered undrained, but rather governs the absolute level of factor of safety. This persistent influence of ϕ' can be attributed to how the frictional component enters the Mohr-Coulomb criterion. Due to the shape of the tangent function in the relevant range of friction angles, a small change in ϕ' produces a relatively large change in tanϕ', which is multiplied by the effective stress along the slip surface, which makes small uncertainties in ϕ' have a large effect on the calculated factor of safety.

5.7 Comparison with Swedish geotechnical recommendations

The excavation geometries analysed in this study were selected based on the recommendations presented in Lundström et al. (2015), where a slope inclination of 1:1 with an excavation depth of 2,75 m is recommended for clay with minimum undrained shear strength of 15 kPa. As presented in Table 4.2, the undrained analysis for this geometry results in a $FoS > 1,5$ which is the requirement according to total stability assessment presented in Figure 2.9 from Skredkommissionen (1995). This confirms that the recommended geometry is appropriate under undrained conditions, and the undrained analysis produces results in line with what would be expected from Swedish practice. However, what should be highlighted is that when performing a combined stability analysis with the material model $Combined, S = f(depth)$ (Method 1), without imported pore pressures, the factor of safety drops to 0,687 which is falling well below the requirements. In contrast, when pore pressure distribution from PLAXIS 2D is imported to SLOPE/W (Method 2), the combined analysis for the factor of safety reaches almost the requirements of 1,3. This difference underscores the importance of accounting for the negative pore pressures that develop immediately after excavation. Neglecting these leads to an underestimation of the short-term stability and may result in overly conservative or misleading assessments of safety of temporary excavations. The results therefore suggest that including time-dependent pore pressure conditions in stability analysis provides a more representative picture of the actual stability, and that the contribution of negative pore pressures should not be disregarded when evaluating the stability of temporary excavations in soft clay.

6

Conclusion and Recommendations

This chapter summarizes the main findings of the study and discusses their implications for the assessment of temporary excavations in soft clay. Based on the results, conclusions are drawn regarding the time-dependent stability behaviour and the applicability of the adopted modelling approach. Recommendations for future research are also presented.

6.1 Conclusion

This thesis investigated the time-dependent slope stability of temporary excavations in soft clay through coupled numerical modelling, combining finite element analyses in PLAXIS 2D with limit equilibrium analyses in SLOPE/W. The study examined how negative pore pressures develop and dissipate following excavation, and how the transient behaviour influences the factor of safety during the transition from undrained to drained conditions.

The results demonstrate that negative excess pore pressures generated by excavation unloading provide a temporary but significant stabilising effect in the short-term. This suction temporarily increases effective stress and shear strength along the critical slip surface, resulting in higher factors of safety immediately after excavation. As consolidation progresses, these pore pressures dissipate and the factor of safety gradually converges towards long-term drained values. This stabilising contribution is real but transient, and should not be relied upon beyond a few days after excavation. By importing time-dependent pore pressure distribution in SLOPE/W, this behaviour could be captured and the stability transition followed step by step throughout the consolidation period.

Slope geometry was found to govern both the magnitude and the rate of the stability transition. Steeper slopes exhibit lower initial factors of safety and reach drained conditions more rapidly. This is because less soil is removed during excavation, resulting in a smaller stress relief and consequently lower negative pore pressures being generated. The critical slip surface is also shallower and closer to the boundaries, reducing both the distance over which pore pressures must dissipate and the total volume of soil affected by suction. In contrast, flatter slopes involve greater stress relief, a deeper slip surface and a larger zone of negative pore pressures that persist for longer before equilibrium is reached. The sensitivity analysis further showed that the effective friction angle is the most critical parameter for stability throughout the consolidation period, influencing both short-term and long-term factors of safety persistently, while Young's modulus and permeability primarily govern the rate of transition rather than the absolute stability level.

Collectively, the findings demonstrate that the transition from undrained to drained conditions is a gradual process that has a significant impact on the stability of temporary excavations in soft clay. Quantifying how long a slope can be considered undrained is not straightforward, and relying solely on an undrained analysis without accounting for the time-dependent pore pressure development risks either overestimating or underestimating stability depending on the stage of consolidation. Integrating time-dependent pore pressure distribution into stability analysis provides a more realistic picture of how safety evolves throughout the open excavation period, and highlights the importance of considering the full undrained to drained transition when assessing the stability of temporary excavations.

6.2 Further work

Several aspects related to temporary excavation behaviour in clay could be investigated further in order to improve the understanding of time-dependent pore pressure development and slope stability. Potential areas for future work include field and laboratory investigations, more advanced numerical modelling approaches and the influence of additional environmental and material-related factors.

A relevant continuation of this work would be to perform a field study investigating pore pressure development and slope stability in connection with excavation under real conditions. The purpose of such a study would be to collect measurements of pore water pressures and deformations that could be compared with the numerical analyses performed in this thesis. Such measurements could be used to evaluate and potentially calibrate the predicted pore pressure development, providing improved understanding of how well the combined analyses represent the time-dependent behaviour of temporary excavations in clay. Future work could also include laboratory testing of unsaturated soil behaviour and determination of ϕ^b, which could improve the representation of suction-related shear strength contributions in the numerical modelling.

The analyses in this study were performed using the Mohr-Coulomb constitutive model, which does not capture stress-dependent stiffness or more advanced soft clay behaviour. Future studies could investigate more advanced constitutive models in PLAXIS 2D. These models incorporate additional material parameters and a more detailed description of soil behaviour, which may influence the predicted pore pressure response and the resulting stability development following excavation. Future work could also investigate fully coupled flow-deformation analyses, where the simultaneous development of deformations and pore pressures is considered directly. Such analyses may provide a more realistic representation of partially drained excavation behaviour and unsaturated soil response. Additionally, it would be of interest to extend the analyses to include additional excavation geometries, such as greater excavation depths, to further investigate how geometry influences the time-dependent pore pressure development and stability.

It would furthermore be relevant to investigate whether similar coupled analyses could be performed using SIGMA/W within GeoStudio, enabling a comparison between different numerical frameworks and modelling approaches. Future studies could also investigate three-dimensional effects using PLAXIS 3D, since real excavations are not fully represented by plane strain conditions and may exhibit additional stabilising effects.

Additional factors that may influence the dissipation of negative pore pressures and the stability development of temporary excavations include soil anisotropy and environmental conditions such as rainfall, evaporation and seasonal groundwater variations. These effects were not considered in this study but could influence both the magnitude and duration of suction in the field.

Bibliography

Abramson, L. W., Lee, T. S., Sharma, S., & Boyce, G. M. (2002). *Slope stability and stabilization methods* (2nd ed.). John Wiley & Sons.

Alén, C., Bengtsson, P.-E., Berggren, B., Johansson, L., Johansson, Å., & Bengtsson, P.-E. (2000). *Skredriskanalys i göta älvdalen-metodbeskrivning* (tech. rep.). Sveriges Geotekniska Institut.

Andrade, F., Al-Qureshi, H., & Hotza, D. (2011). Measuring the plasticity of clays: A review. *Applied Clay Science*, *51*(1), 1–7. https://doi.org/10.1016/j.clay.2010.10.028

Bentley Systems. (2025a, November). *PLAXIS 2D 2025.1 Materials Models Manual* (tech. rep.). SEEQUENT.

Bentley Systems. (2025b, November). *PLAXIS 2D 2025.1 Reference Manual* (tech. rep.). SEEQUENT.

Bishop, A. W. (1954). *First technical session : General theory of stability of slopes the use of the slip circle in the stability analysis of slopes* (tech. rep.).

Craig, R. F. (2004). *Craig's soil mechanics, seventh edition* (Seventh). Taylor & Francis Group.

Eigenbrod, K. D. (1974). Analysis of the pore pressure changes following the excavation of a slope. *Canadian Geotechnical Journal*, *12*, 429–440.

Fredlund, D. G. (1989). *Negative pore-water pressure in slope stability* (tech. rep.). University of Saskatchewan.

Fredlund, D. G., & Vanapalli, S. K. (2002). Shear strength of unsaturated soils. In *Methods of soil analysis: Part 4 physical methods* (pp. 329–361). Soil Science Society of America. https://doi.org/10.2136/sssabookser5.4

IEG. (2008). *Tillämpningsdokument en 1997-1 kapitel 11 och 12: Slänter och bankar rapport 6:2008 rev 1* (tech. rep.). (Implementeringskommission för Europastandarder inom Geoteknik. www.ieg.nu

Karstunen, M., & Amavasai, A. (2017). *Best soil: Soft soil modelling and parameter determination* (tech. rep.). Chalmers University of Technology.

Knappett, J. A., & Craig, R. F. (2012). *Craig's soil mechanics* (Eighth). Spon Press.

Larsson, R. (1983). *Släntstabilitetsberäkningar i lera* (tech. rep.). Sveriges Geotekniska Institution.

Larsson, R. (2008). *Jords egenskaper* (tech. rep.). Statens Geotekniska Institut (SGI).

Larsson, R., Sällfors, G., Bengtsson, P.-E., Alén, C., Bergdahl, U., & Eriksson, L. (2007). *Skjuvhållfasthet - utvärdering i kohesionsjord* (tech. rep.). Statens Geotekniska Institut (SGI).

Lundström, K., Odén, K., & Rankka, W. (2015, May). *Schakta säkert säkerhet vid schaktning i jord* (tech. rep.). www.byggtjanst.se

Rajamanthri, K., & Zapata, C. E. (2025). A non-linear suction-dependent model for predicting unsaturated shear strength. *Geosciences*, *16*, 12. https://doi.org/10.3390/geosciences16010012

Sabattini, M., Hall, L., Ekstrand, D., & Thorén, T. (2024, August). *Temporära slänter fördjupningsbilaga till SGI vägledning 8 utredning av släntstabilitet. sbuf-projekt: 13957* (tech. rep.). Statens Geotekniska Institut.

Sällfors, G. (2013). *Geoteknik* (Fifth Edition). Cremona Förlag.

Seequent. (n.d.). *Geostudio example file material model: Shear normal function geostudio example-material model: Shear normal function* (tech. rep.). Seequent.

Seequent. (2022). *Stability modeling with geostudio* (tech. rep.). Seequent Limited.

Seequent. (2025). *Slope stability modeling* (tech. rep.). Seequent limited.

SGI. (2023, June). *Utredning av släntstabilitet Utgåva 1* (tech. rep.). Sveriges Geotekniska Institut.

Skredkommissionen. (1995). *Anvisningar för släntstabilitetsutredningar* (tech. rep.). INGENJÖRSVETENSKAPSAKADEMIEN.

Terzaghi, K. (1943). *Theoretical soil mechanics*. John Wiley & Sons.

Tornborg, J. (2024). *On the temporal evolution of earth pressures in deep excavations in soft clay* [Doctoral thesis]. Chalmers University of Technology.

Trafikverket. (2011, June). *Trafikverkets tekniska krav för geokonstruktioner*.

Verruijt, A. (2017). *An introduction to soil mechanics*. Springer International Publishing. https://doi.org/10.1007/978-3-319-61185-3

VJ Tech. (2024). *An introduction to unsaturated testing* [Accessed: 2026-05-07]. https://www.vjtech.co.uk/an-introduction-to-unsaturated-testing/

Wu, T. H., & Kraft, L. M. (1970). Safety analysis of slopes. *Journal of the Soil Mechanics and Foundations Division*, *96*(2), 609–630. https://doi.org/10.1061/JSFEAQ.0001406

A

Appendix: Mesh

This Appendix presents the chosen mesh for the three different slope geometries from PLAXIS 2D.

A.1 Slope inclination 1:1

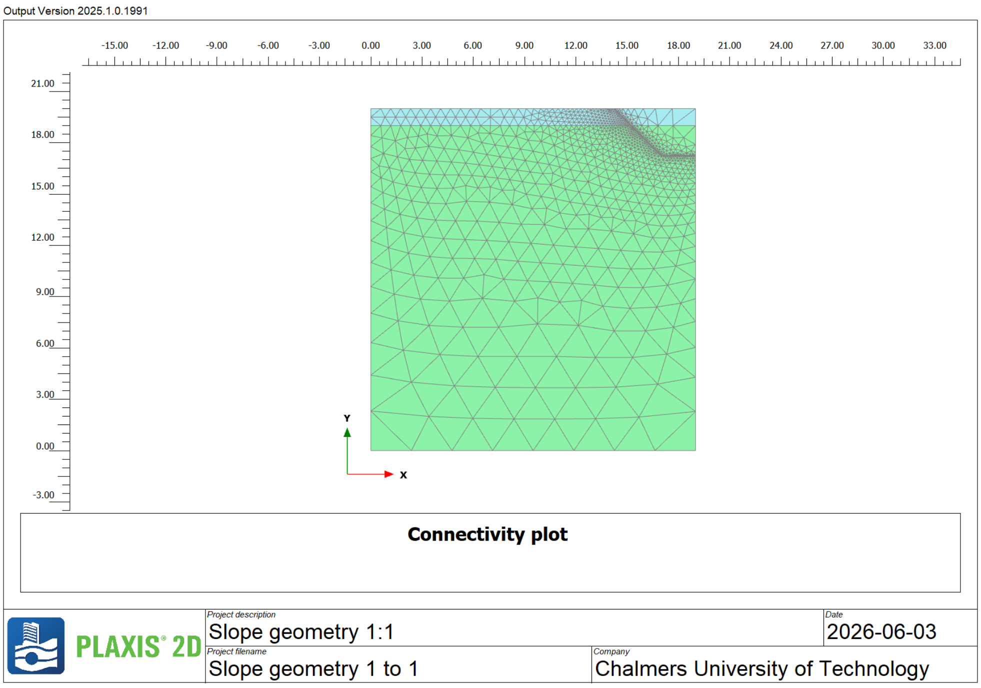

Figure A.1: Final mesh for the slope geometry 1:1 with excavation depth H=2,75 m.

A.2 Slope inclination 1:1,5

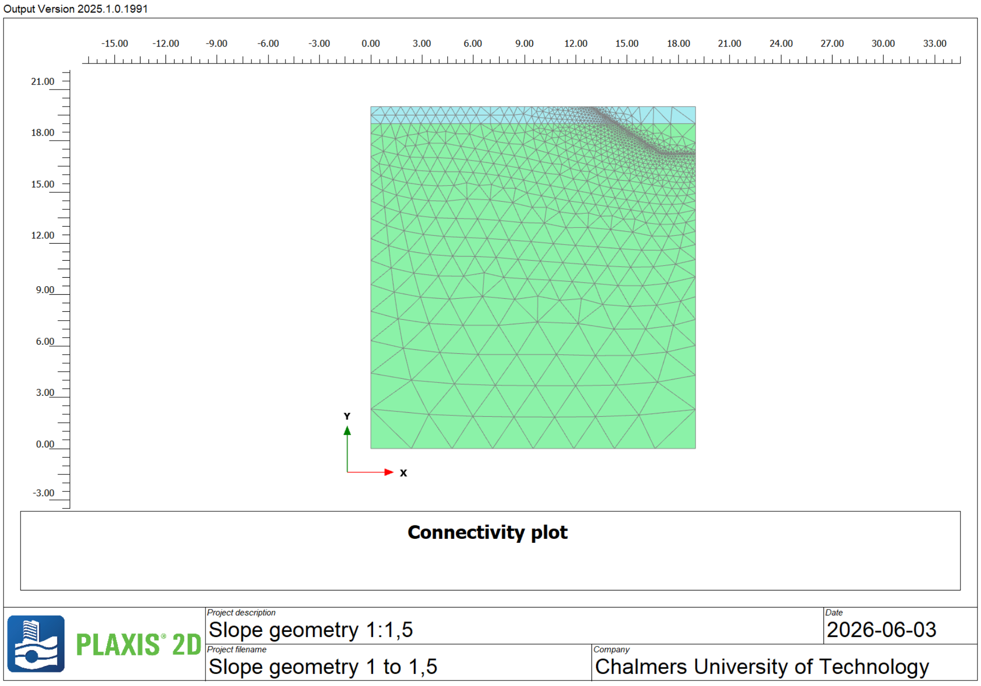

Figure A.2: Final mesh for the slope geometry 1:1,5 with excavation depth H=2,75 m.

A.3 Slope inclination 1:2

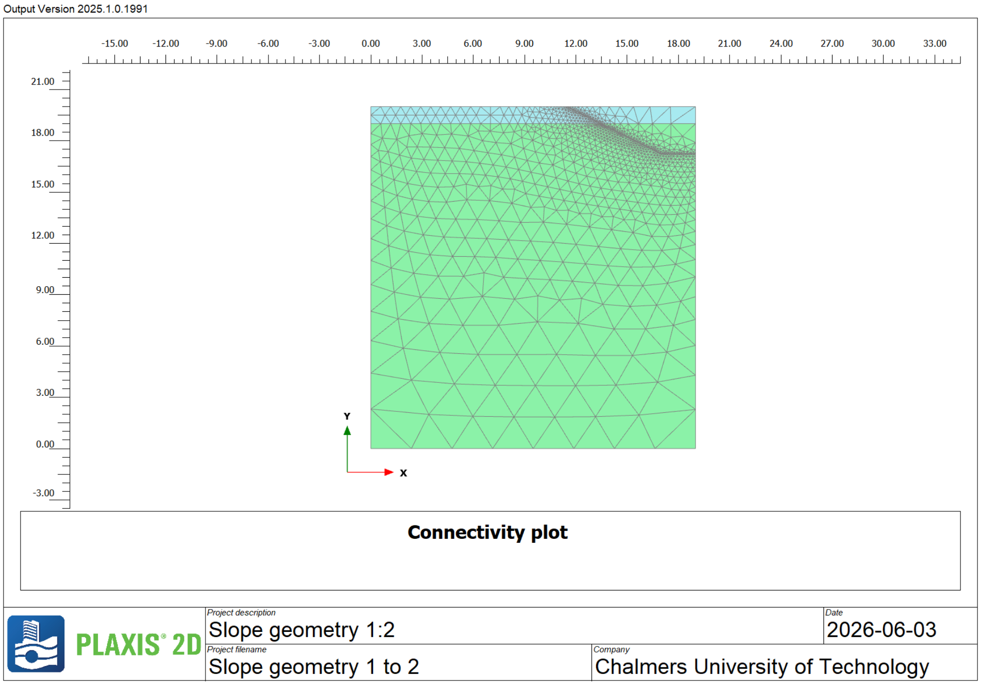

Figure A.3: Final mesh for the slope geometry 1:2 with excavation depth H=2,75 m.

B

Appendix: Analysed time steps for each slope geometry

Table B.1 summarises the analysed time steps for each slope geometry. Since the rate of pore pressure dissipation differed between the geometries, different time intervals were selected to capture the transition from undrained to drained conditions. The analyses were continued until the factor of safety approached the fully drained factor of safety and only negligible changes occurred between consecutive time steps.

Table B.1: Analysed time steps for each slope geometry.

Time after excavation [days]	Slope 1:1	Slope 1:1.5	Slope 1:2
1	x	x	x
5	x	x	x
10	x	x	x
15	x	x	x
20	x	x	x
35	x	x	x
50	x	x	x
70	x	x	x
100	x	x	x
120	x	x	x
140	x	x	x
150	x	x	x
160		x	x
180		x	x
200		x	x
240		x	x
280		x	x
300		x	x
400			x
500			x

C

Appendix: Pore Pressure Distributions

This appendix presents the complete pore pressure distributions in SLOPE/W used in the analysis. The figures show the development of pore pressure over time for the three studied excavation geometries. For each geometry, the pore pressure distribution is shown at selected time steps after excavation.

C.1 Slope inclination 1:1

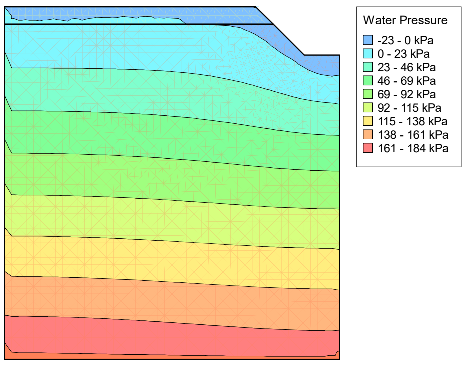

Figure C.1: Pore pressure distribution for slope inclination 1:1 at 1 day after excavation.

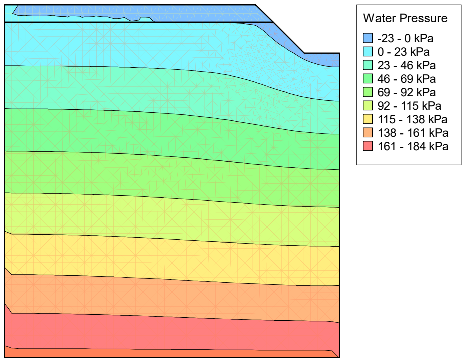

Figure C.2: Pore pressure distribution for slope inclination 1:1 at 50 days after excavation.

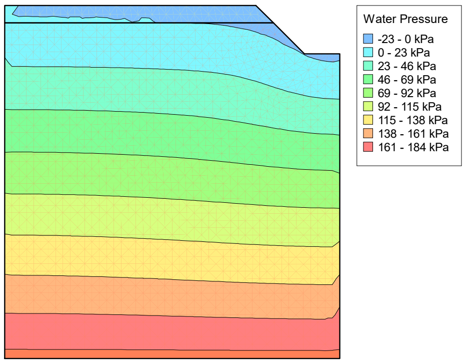

Figure C.3: Pore pressure distribution for slope inclination 1:1 at 150 days after excavation.

C.2 Slope inclination 1:1.5

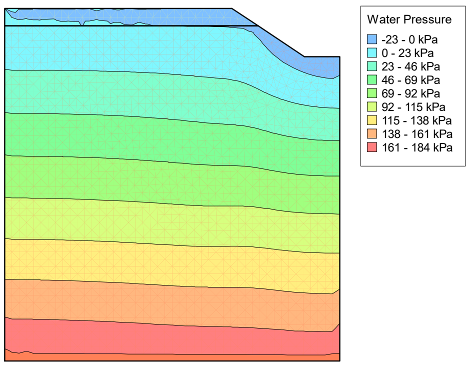

Figure C.4: Pore pressure distribution for slope inclination 1:1.5 at 1 day after excavation.

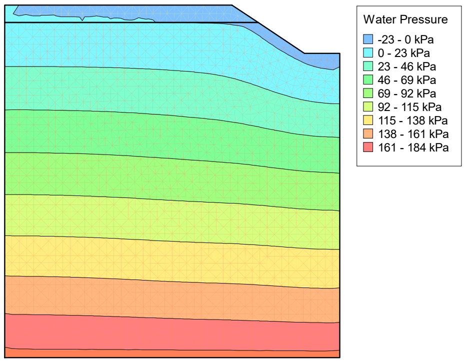

Figure C.5: Pore pressure distribution for slope inclination 1:1.5 at 50 days after excavation.

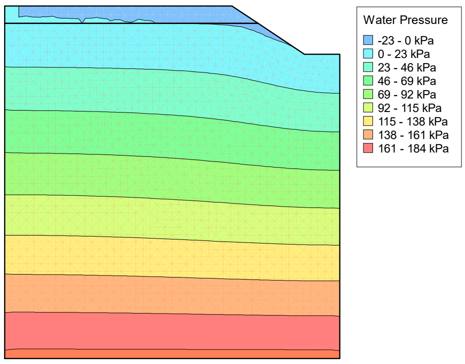

Figure C.6: Pore pressure distribution for slope inclination 1:1.5 at 300 days after excavation.

C.3 Slope inclination 1:2

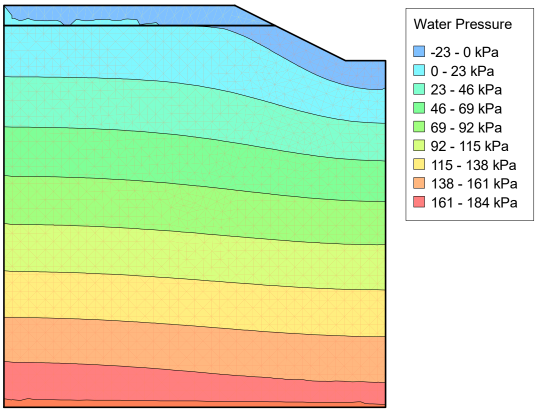

Figure C.7: Pore pressure distribution for slope inclination 1:2 at 1 day after excavation.

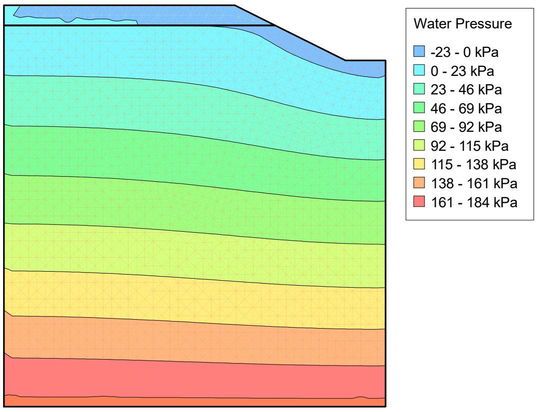

Figure C.8: Pore pressure distribution for slope inclination 1:2 at 100 days after excavation.

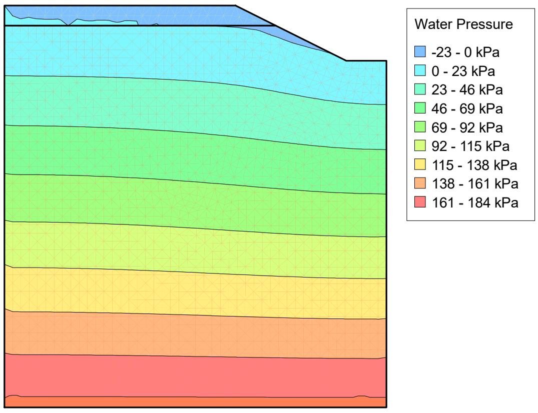

Figure C.9: Pore pressure distribution for slope inclination 1:2 at 500 days after excavation.

D

Appendix: Additional analysis of the 1:2 slope geometry

Appendix D presents an additional analysis for the 1:2 slope geometry where the undrained shear strength, c_u, was increased from 15 kPa to 16 kPa in the Shear/Normal Function approach. The increase in undrained shear strength resulted in a shallower critical slip surface, as illustrated in Figure D.2. Furthermore, the shear resistance distribution along the slip surface shown in Figure D.1 indicates that the shear resistance gradually decreases with time after excavation along the entire slip surface. Compared to the original analysis, the higher c_u value increased the overall shear resistance level and contributed to a higher factor of safety for the slope.

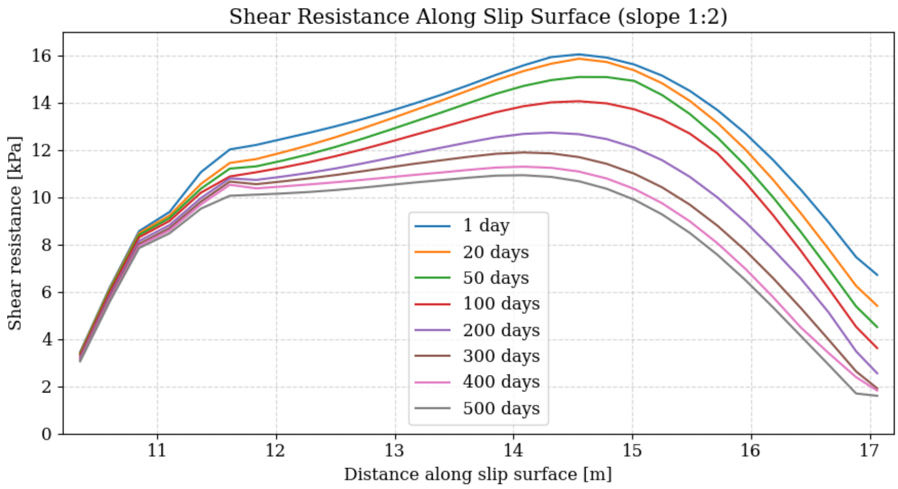

Figure D.1: The shear resistance along the slip surface corresponds to the critical slip surface identified 1 day after excavation.

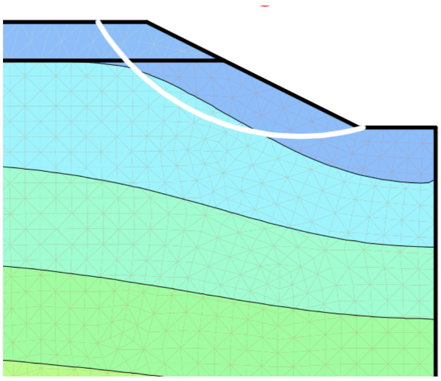

Figure D.2: Critical slip surface identified at 1 day after excavation.

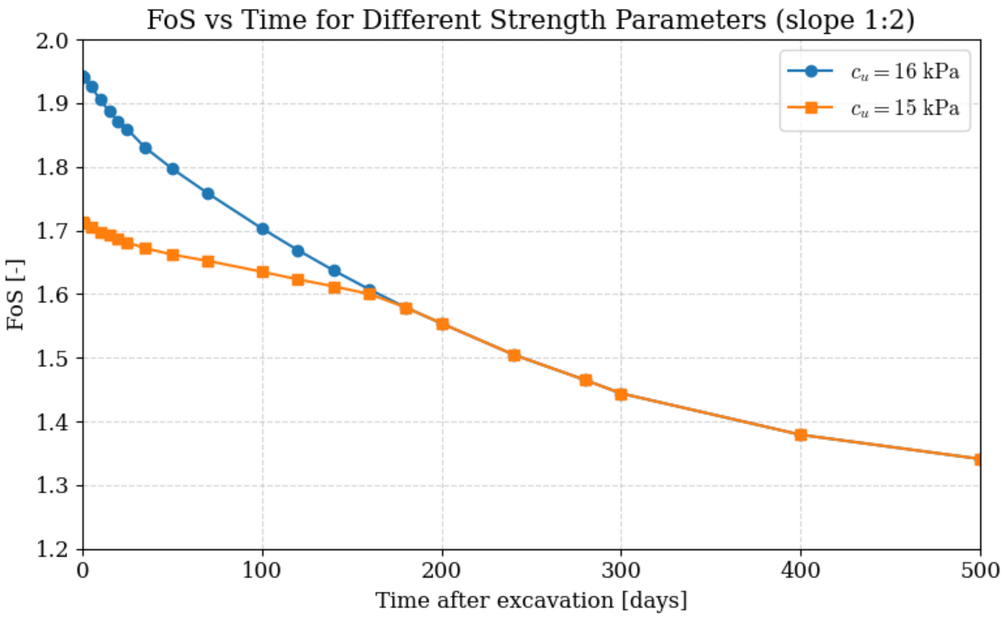

Figure D.3: Comparison slope 1:2 with c_u = 15 kPa and c_u = 16 kPa.

DEPARTMENT OF ARCHITECTURE AND CIVIL ENGINEERING
CHALMERS UNIVERSITY OF TECHNOLOGY
Gothenburg, Sweden
www.chalmers.se

CHALMERS
UNIVERSITY OF TECHNOLOGY